MASTERARBEIT | MASTER'S THESIS

Titel | Title

KompotSpec - Planetary Atmosphere Simulations

verfasst von | submitted by

Andreas Cyniburk BSc

angestrebter akademischer Grad | in partial fulfilment of the requirements for the degree of

Master of Science (MSc)

Wien | Vienna, 2025

Studienkennzahl lt. Studienblatt | Degree programme code as it appears on the student record sheet:	UA 066 861
Studienrichtung lt. Studienblatt | Degree programme as it appears on the student record sheet:	Masterstudium Astronomie
Betreut von | Supervisor:	Ass.-Prof. Dr. Sudeshna Boro Saikia

Acknowledgments

This work marks the end of the road for my journey through the educational system (for now, at least). In these past two decades of my life many things have happened; some good, some less so. However, there were also those who helped me to stay on the right path *...or at least helped me find it again.* To see the end of the tunnel. Now, at the end of the proverbial tunnel, I want to express my gratitude to you.

First and foremost, I want to thank my parents *Bernhard* and *Natallia*. In the 23 years we've lived under the same roof you've taken care of me, listened to me ramble about my interests, but also about my sorrows. You've also encouraged my curiosity about all kinds of subjects. And even though you were not exactly sold on my choice of university degree at first, you eventually came around and supported me anyway. Both mentally as well as financially when it came time for me to move out and fend for myself. Now that I am truly an independent adult, I want you to know that I understand the gift you've given me. Here's to many more years together, in good health.

I also want to thank my dear family, for all the same reasons.

Jan, our friendship is the longest-lasting one I've ever had. And still, despite both of us being working adults now, it somehow still feels like we're kids. I'm not sure if that will ever stop, and even less sure whether I'd even want it to. What I am sure about is that I'm glad to be your friend and look forward to what the future holds.

Schanz, although we were not friends at first sight, I still had one hell of a time with you during school. When we were working or learning long nights, but also when we were just having fun. You were the one who gave me the idea to study Astronomy. I've never regretted walking this way with you, and I am excited to see where our lives will lead us in the years to come.

Also thanks to everyone who worked through endless courses and lectures with me. *Schanz*, again, and *Thomas*: You've worked with me on untold numbers of assignments, helped me learn for exams whenever I'd waited until the last minute (*as usual*) and been valuable friends and colleagues all throughout our academic journey. But also to *Hannah*, *Mali*, *Petra*, *Michi*, *Kerschi*, *Mary* and everyone else. To all of you, I want to say: I couldn't have done it without you.

Everyone I've had the pleasure of working with at the VHS planetarium and observatories: Thank you for being wonderful people, sharing your excitement with me and letting me share mine. Getting paid to share things I am passionate about is truly an incredible experience. It also transformed my stage fright from years past, and made me realize that I actually enjoy talking and performing in front of an audience.

Last, but not least, thank you *Jasmin*. In the short time we've known each other, you've enriched my life in so many ways I didn't even know were possible. Thank you for helping with this work, both for giving me motivation to work when I really needed it and for distracting me from it when necessary. I can't imagine anyone I'd rather spend my time with, and I'm looking forward to our next adventures together.

Thanks to everyone of you for making all this possible,
Andreas

Abstract

Measuring exoplanetary atmospheres via transit spectroscopy is a fundamental step to a good understanding of planetary evolution and possible habitability. Atmospheric models can be used to infer atmospheric parameters, based on observational data, by producing synthetic transit spectra. Kompot, the model featured in this thesis, did not have the capability to produce these.

This thesis introduces KompotSpec, an extension to the Kompot code able to generate synthetic transit spectra from Kompot simulation results in various wavelength ranges, including UV and IR wavelengths for comparison with observations. KompotSpec takes atmospheric profiles from Kompot, generalizes them and computes wavelength-dependent optical depths, using UV crosssections available in Kompot and IR crosssections from the ExoMolOP database. For comparison, KompotSpec's synthetic transit spectra are contrasted with observed transit spectra of Earth and Titan in this work.

The synthetic transit spectra produced by KompotSpec successfully reproduce major absorption features in both Earth's and Titan's atmospheres. However, some minor absorbers can not be reproduced by KompotSpec, and the lack of pressure broadening effects complicates comparison with observational data. Nonetheless KompotSpec finally provides significant enhancements to the Kompot model, enabling the comparison of its detailed atmospheric photochemical models with IR observational data. With its initial results, further improvements like inclusion of pressure broadening and performance optimizations will make interpretation of transit spectra and retrieval of atmospheric constituents using Kompot easier than before.

Kurzfassung

Exoplanetenatmosphären mittels Transitspektroskopie zu beobachten ist essenziell um die Evolution von Planeten und ihren Atmosphären, als auch potenzielle Habitabilität zu verstehen. Atmosphärische Modelle können dazu verwendet werden, atmosphärische Eigenschaften von Beobachtungsdaten abzuleiten, indem Sie synthetische Transitspektra erzeugen. Kompot, das in dieser Arbeit verwendete Modell, hatte jedoch bisher nicht die Fähigkeit diese synthetischen Spektra zu produzieren.

Diese Arbeit führt KompotSpec ein, eine Erweiterung des Kompot Codes, welche es ermöglicht synthetische Spektra aus Kompot Simulationsergebnissen in verschiedenen Wellenlängen (zB. UV und IR) zu produzieren. KompotSpec verwendet Kompot's Atmosphärenprofile, generalisiert sie und berechnet wellenlängenabhängige optische Tiefen und Transittiefen, mithilfe von den in Kompot vorhandenen UV Crossections und IR Crosssections der ExoMolOP Datenbank. KompotSpec's synthetische Transitspektra werden abschließend außerdem mit beobachteten Transitspektra von der Erde und von Titan verglichen.

Die synthetischen Transitspektra von KompotSpec reproduzieren erfolgreich die Haupt-Absorptionsfeatures, sowohl in der Atmosphäre der Erde als auch der von Titan. Jedoch können einige der kleineren Absorptionsfeatures nicht reproduziert werden, und das Fehlen von Pressure Broadening verkompliziert den Vergleich mit Beobachtungsdaten. Trotzdem macht es KompotSpec nun möglich Kompot's detaillierte photochemischen Atmosphärenmodelle mit IR Beobachtungsdaten zu vergleichen. Mit den ersten Ergebnissen ist absehbar das mit weiteren Verbesserungen (wie Pressure Broadening und besserer Performance) die Interpretation von Transitspektra und atmosphärischen Eigenschaften mittels Kompot einfacher als zuvor wird.

Contents

List of Tables

List of Figures

1. Introduction

Soon after the discovery of planets outside our own solar system, exoplanets, the study of their atmospheres quickly gathered interest. By using instruments to create transit spectra of their atmospheres, atmospheric characterization became possible. Matching atmospheric models to the observations enables us to determine atmospheric properties of planets unlike the well-studies planets of our own solar system. The diversity in planet types, atmospheres and models is however great and study of each of those areas is necessary.

1.1. Exoplanets

1.1.1. Discovery methods

Exoplanets were long considered a theoretical idea, until the 1990s when their existence was confirmed. Wolszczan and Frail (1992) discovered planets orbiting pulsar *PSR B1257+12* using the pulsar timing method. But this detection, due to the extreme nature of the host star, was soon overshadowed by Mayor and Queloz (1995). Using Doppler shift measurements, also called the Radial Velocity (RV) method, they were able to measure masses of exoplanets for the first time. With the RV method, they found the first exoplanet around a main sequence star, *51 Pegasi b*, a planet dwarfing Jupiter in size while orbiting its host star very closely. This breakthrough revealed how exoplanets could differ significantly from those in our solar system.

Soon afterwards the transit method became pivotal for exoplanet detection, with examples like *HD 209458 b* observed by Charbonneau et al. (2000) and Henry et al. (2000). By measuring the dimming of the combined planet-star system such as in Figure 1.1, it is possible to detect planets and measure their radius (if the stellar radius is known). Combined with RV measurements for mass, this allows the mean density to be calculated.

1.1.2. Types and demographics of exoplanets

The currently known population of exoplanets can be broadly divided into three categories. The first category are Sub-Jovians and Jovians, planets larger than 3.5 $R_\oplus$ with significant amounts of gas (and ice for Sub-Jovians). Terrestrial planets roughly around one $R_\oplus$ sit at the other end of the spectrum, being composed mostly of solids. The gap in between 1 and 3.5 $R_\oplus$ is taken up by intermediate-sized planets which we will collectively call Sub-Neptunes. These planets can vary significantly in composition and are not very well

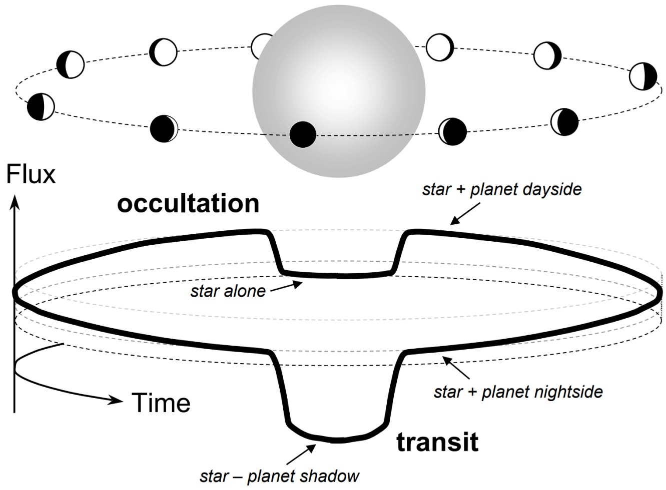

Figure 1.1.: An exoplanet transiting its host star (Top) and the resulting lightcurve of the system (Bottom), Source: Winn (2014)

understood currently. Figure 1.2 shows the current exoplanet size distribution. The most numerous planets are Sub-Neptunes around two $R_\oplus$, while few planets below 1 $R_\oplus$ have been discovered. Of note is that this plot contains all confirmed exoplanets with available radii, meaning practically all of those will have been measured via the transit method.

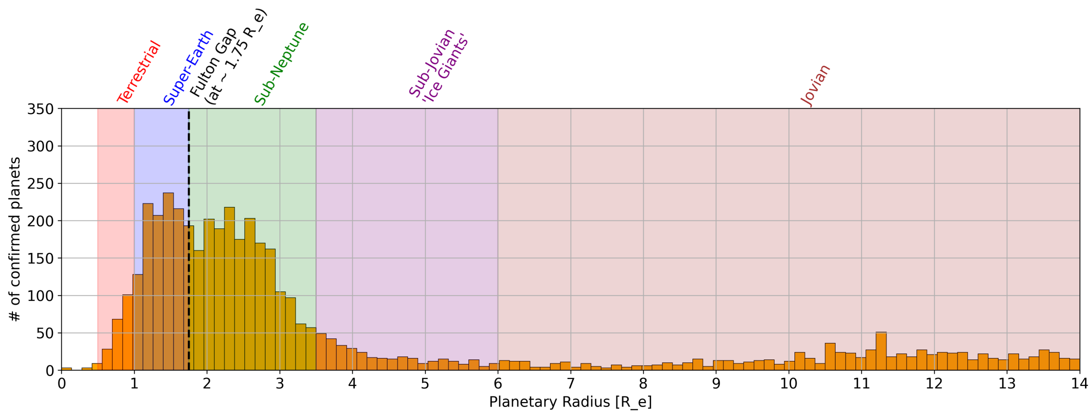

Figure 1.2.: Exoplanet type demographics; Radius definitions used from NASA Exoplanet Modeling and Analysis Center; Data used from Encyclopaedia of exoplanetary systems

The distinction between smaller rockier Sub-Neptunes and Sub-Neptunes of other compositions is however complicated. As can be seen in Figure 1.3, where observed exoplanets with orbital periods less than 100 days are shown, it is not a uniform distribution but instead a distribution with two peaks/sub-populations. This 'radius valley' (or 'Fulton

Gap') is not fully explained, but there are theories to explain the radius valley:

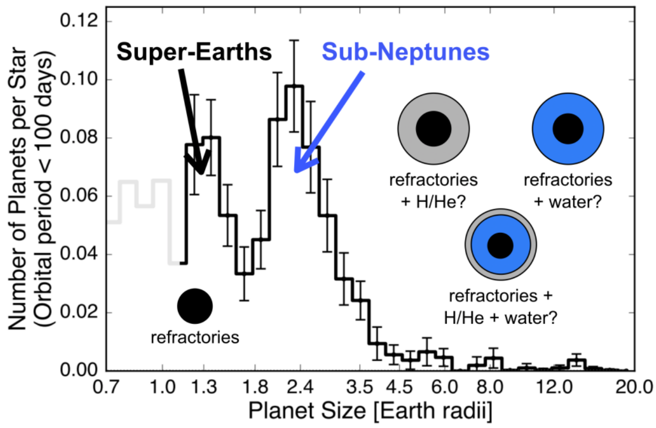

Figure 1.3.: Distribution of close-in exoplanets (orbital period smaller than 100 days); Two different peaks for rocky Sub-Neptunes ("Super-Earths") and Sub-Neptunes of other compositions with the so-called radius valley in between; Source: Cloutier (2024); 'refractories' refers to bulk composition of refractory materials such as iron or silicates

- Photoevaporation processes driving atmospheric mass loss (Owen and Wu, 2013; Fulton et al., 2017) with certain atmosphere-to-core radius ratios being less susceptible to photoevaporation (Owen and Wu, 2017)
- Runaway gas accretion by the larger planets (Venturini and Helled, 2017)
- Observational bias towards hot planets with extended atmospheres (Mousis et al., 2020)

The processes behind the radius valley complicate the classification of Sub-Neptunes. Figure 1.3 shows that Sub-Neptunes can have widely varying compositions (some of them listed in Subsection 1.2.3) yet similar mean densities, which are currently the only measurable parameter. Additional challenges include not having a Sub-Neptune analogue in our own solar system, making validation of exoplanet measurements harder. Determining whether a planet has a gaseous envelope, is covered in water, or something in between requires detailed atmospheric characterization (such as modeling the atmosphere).

1.2. Atmospheric detection & characterization

The first detection of an exoplanetary atmosphere around *HD 209458 b* was made by Charbonneau et al. (2002), identifying Na via its strong absorption feature in the visible wavelength spectrum. Since then, various instruments have detected other atmospheric constituents, including H_2O, CO, CO_2, and CH_4 around *HD 189733 b* (Swain et al., 2008), notably using HST's NICMOS instrument in the infrared wavelength. Fraine et al. (2014) later identified water vapor in *HAT-P-11b*, a Neptune-sized exoplanet, using combined data from HST's WFC3 and Spitzer's IRAC instruments. Tsiaras et al. (2019) also detected water vapor around *K2-18b*, a habitable-zone exoplanet. Though this discovery is controversial, with some claiming this to be implausible from modeling (Blain et al., 2021), and later re-observations with the James Webb Space Telescope (JWST) finding very low concentrations of water vapor (Madhusudhan et al., 2023). While these discoveries relied on instruments not specifically designed for atmospheric studies, the launch of the JWST in 2021 revolutionized the field by providing high-resolution infrared spectroscopy and confirming water vapor in *WASP-96b*'s atmosphere (Taylor et al., 2023) using its Near Infrared Imager and Slitless Spectrograph (NIRISS) instrument (Doyon et al., 2023). CO_2 and SO_2 were also found in gas giant *WASP-39b* for the first time (Ahrer et al., 2022; Tsai et al., 2023) indicating photochemistry with the Near-Infrared Spectrograph (NIRSpec) instrument (Jakobsen et al., 2022).

There are also results for some smaller planets, however they are much less conclusive. One such case is the spectrum of *GJ 1214 b*, a Sub-Neptune, which is considered featureless (Bean et al., 2010). The authors manage to rule out cloud-free hydrogen atmospheres with high confidence, however find that either a cloudy hydrogen atmosphere or dense water vapor atmosphere could reproduce the spectrum. Another case is *TRAPPIST-1 c* which was studied using emission spectroscopy from JWST (Zieba et al., 2023), finding no dense CO_2 or O_2 atmosphere. Despite this, either no atmosphere or thinner atmospheres could still explain the gathered data. The latter case of *TRAPPIST-1 c* illustrates the difficulties of measuring atmospheres of rocky exoplanets. The planets are both smaller, making them harder to detect against the host star, but also typically have smaller, less dense atmospheres than the larger gaseous planets. Both cases however show that observations are alone are not always enough to characterize an atmosphere, and understanding of atmospheric evolution is necessary.

1.2.1. Atmospheric properties of gaseous planets

Gaseous exoplanets (analogous to our own Jupiter and Saturn) consist mainly of a thick H and He envelope. Other elements and metallicity of each planet can vary (but can include H_2O, CO_2, CH_4). Distance to the host star also influences atmospheric properties: hot Jupiters are a common class of gaseous exoplanet, which orbit closely to their star (typically orbital periods less than ten days) and therefore feature more irradiated atmospheres. Typical is that they are often tidally locked to their star due to the close proximity (Mendonça, 2019), and that atmospheres can feature supersonic winds and storms (Cooper and Showman, 2005). Some Hot Jupiters also have clouds/hazes (Sing et al., 2015) in their atmospheres, which can obscure other features and make atmospheric characterization difficult.

1.2.2. Atmospheric properties of rocky planets

Less of a blanket statement can be made for atmospheric properties of rocky exoplanets. While many rocky exoplanets, especially around red dwarfs, might not have a significant atmosphere due to severe atmospheric stripping via XUV radiation (as argued for *TRAPPIST-1* in Van Looveren et al. (2024)), others such as *55 Cancri e* (Hu et al., 2024) have JWST observations consistent with thick atmospheres.

Unlike with gaseous exoplanets, it is much harder to conclusively assert the presence of an atmosphere. This is in part because the relative size of these planets compared to their star makes their atmospheres harder to measure. Often measurement quality only suffices to rule out thick H and He envelopes, without the ability to discern a thin planetary atmosphere from no atmosphere at all (such as in *GJ 1132 b* using JWST data (Xue et al., 2024) and *LHS 3844b* (Diamond-Lowe et al., 2020), both emission spectroscopy measurements). Formation of clouds/hazes is also possible further complicating atmospheric characterization of rocky exoplanets.

1.2.3. Atmospheric properties of Sub-Neptunes

The mean densities of exoplanets, derived from transit and radial velocity methods, can indicate rocky or gaseous compositions. However, most exoplanets fall between these extremes, where mean density alone cannot reveal their interior composition. Figure 1.3 shows a bimodality in close-in exoplanets. The rocky Sub-Neptunes are smaller and feature mean densities similar to rocky planets and their atmospheric properties are also thought to be quite similar.

For other Sub-Neptunes this is not the case. Their densities could be consistent with a multitude of interior compositions. Current theories include worlds with extensive amounts of water or ice (Zeng et al., 2019) or a rocky core, shell and on top of that a magma ocean (Misener et al. (2023) Kite et al. (2020)). And while opinions differ regarding core compositions, the common thread is that a very voluminous H_2 atmosphere is necessary. By some estimates a few percent of the planet's mass are needed to explain the planet's density for such large radii (Lopez and Fortney, 2014). In addition to H_2 Misener et al. (2023) (who describes the scenario of a magma-ocean Sub-Neptune) expects to see significant amounts of silane and water vapor, produced by reactions of sulfate, oxygen and hydrogen species. Through interactions with the magma ocean, silicon products from the magma ocean could escape into the atmosphere. Potentially allowing one to place constraints on the planet's interior by measuring it's atmospheric composition.

JWST results for Sub-Neptunes are also available, Holmberg, Måns and Madhusudhan, Nikku (2024) investigating *TOI-270 d* and suggesting it to be a candidate for a planet covered by an ocean. *K2-18b* was also observed using JWST with interpretations ranging from another planet-wide ocean (Madhusudhan et al., 2023) to a magma ocean (Shorttle et al., 2024) based on the same data.

1.2.4. Transit & emission spectroscopy

The techniques used for these measurements are called transit spectroscopy and emission spectroscopy. The former involves measuring the band of atmosphere visible during transit in Figure 1.1 using a spectrograph. The latter also uses a spectrograph but measures the nearly fully illuminated side of the planet shortly before/after the occultation (also called secondary eclipse) in Figure 1.1. Looking at the transiting planet via a spectrometer, it is possible to measure the transit depth of the planet in different wavelengths. A transit spectrum is shown in Figure 1.4 from Sarkar et al. (2024), where on the x-axis the observed wavelength (corresponding to the pixel position on the detector) usually given in units of nm, μm, or Angström (Å)[1]. On the y-axis of Figure 1.4 we have the transit depth, also commonly given in percent or parts-per-million (ppm). A planet without an atmosphere would produce (barring any other complications) a constant transit-depth for every measured wavelength. As can clearly be inferred from the measured data (black errorbars with color of central dot indicating used instrument) *WASP-39b* does indeed seem to have an atmosphere, which is supported by the orange line (which represents an atmospheric model).

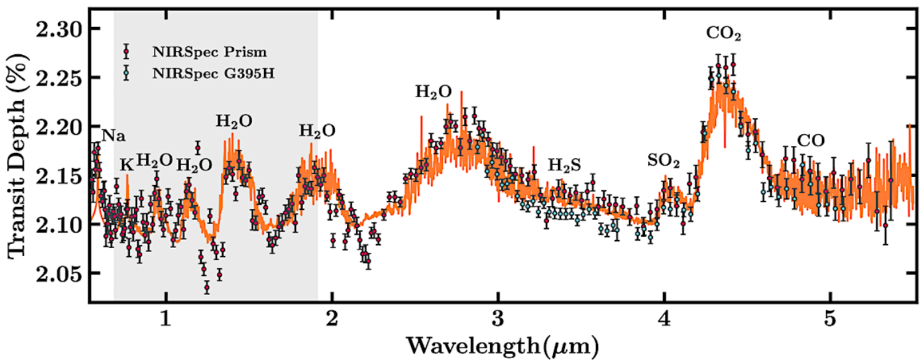

Figure 1.4.: Transit spectrum of *WASP-39b*, measurements in black, Orange line: atmospheric model, Source: Sarkar et al. (2024)

1.2.5. Planetary atmospheric evolution

Planets form from protoplanetary disks which are composed of around 99% gas, the remainder of that being dust (Williams and Cieza, 2011). Gravitation, magnetic fields and other instabilities lead to the collapse of the protoplanetary disks into planetesimals,

[1] As a note for future chapters, this can also be expressed as energy (in units of eV for example) on the x-axis combining the formulas $E = h\nu$ and $\nu = \frac{c}{\lambda}$ to $E = \frac{hc}{\lambda}$ to convert wavelength to energy.

planetary embryos and finally planets. Depending on the planetary type further atmospheric evolution diverges.

Atmosphere formation

Gaseous planets and their precursors, owing to their strong gravitation and the not-yet dissipated gaseous protoplanetary disk, accrete lots of gas quickly (independent of considered planetary formation model). Accretion effectively ends once the disk is depleted which happens after around 10 Myrs (Li and Xiao, 2016) for Sun-like stars. The planet and atmosphere then cool and contract, shedding some of the heat from the accretion process. Whether the gas planet is close to its star, like a hot Jupiter, will also influence its final atmospheric composition.

For rocky planets a hot planetary surface / magma ocean remains after accretion from the disk is finished and the initial gaseous envelope has dissipated. The previously light, gaseous atmosphere is altered by the magma ocean depositing volatiles into the atmosphere (Wordsworth and Kreidberg, 2022). The duration of this stage is governed by the principal heat sources of planets (both gaseous and rocky): energy deposited into the planet from the accretion process (Ransford, 1982), radioactive decay of the elements within the planetary cores (O'Neill et al., 2020) and tidal heating from orbital eccentricity or companions (Jackson et al., 2008).

Once the planets cools sufficiently, the magma ocean eventually freezes, after which further outgassing primarily occurs from volcanic activity (Wordsworth and Kreidberg, 2022). This signifies the last stage of evolution of the atmosphere, which is now further shaped by stripping processes.

1.2.6. Stripping of atmospheres

Some of the most relevant stripping processes, affecting both atmospheres of rocky and gaseous planets include thermal escape mechanisms such as core powered loss, where heat from the planetary core drives escape (Gupta and Schlichting, 2019) or XUV-driven atmospheric escape from the host star's XUV radiation (Sanz-Forcada, J. et al., 2011). Impacts of large objects / planetesimals can additionally cause atmospheric loss (Schlichting and Mukhopadhyay, 2018). Other non-thermal loss processes such as photochemical escape (Shematovich and Marov, 2018), where high energy UV photons break apart molecules making their constituents fast enough to escape, or sputtering (Lundin et al., 2007), which imparts excess energy of the stellar wind to atmospheric constituents, also contribute to stripping of atmospheres. For this work the XUV-driven escape is most significant (and more generally the influence of the host star). Stellar irradiation is also subject to change over time, not only due to the protostar maturing to the main sequence, but also due to stellar variability and different spectral types evolving differently over their stellar lifetimes.

Influence of the host star

The host star has an enormous importance in the evolution of exoplanets and their atmospheres. Not only do the contents of the molecular cloud, which fuel both the stellar and planetary makeup of the resulting system, kick off the formation of the planetary system. But also both stellar evolution and irradiation affect how an exoplanetary atmosphere evolves. This is true for the entire lifetime of the planet and its atmosphere. Irradiation is especially important in the short wavelength regime such as the XUV, which plays a big role in atmospheric escape. This is because photons in this energy range have the following effects on an atmosphere: XUV photons heat up the atmosphere (Sanz-Forcada et al., 2011), thereby expanding it and making easier to strip. They can also break down such as H_2O or CO_2, causing molecular dissociation and production of reactive species thereby altering the atmospheric composition and reactions (Maggio et al., 2024). Generally the XUV evolution of the atmosphere is coupled to the XUV evolution of the star, which is summarized in Appendix A.

1.3. Atmospheric simulations

Previous research (especially in Sub-Neptune atmospheres) has shown observations by itself to be insufficient to understand exoplanetary atmospheres. Especially since various planetary, stellar and atmospheric processes combined are hard to interpret from observations alone. Planetary and stellar properties have to be taken into account when modeling an exoplanetary atmosphere. Planetary parameters include mass and radius, which determine the gravity and scale height of the atmosphere, and as such how easily an atmosphere can escape to space. Composition and interior structure are also important. Stellar parameters such as spectral type also alter the spectrum, which influences the XUV irradiation, which again changes the photochemistry happening inside the atmosphere. Our understanding can therefore be improved by coupling atmospheric models to observations.

1.3.1. Modeling

TRAPPIST-1 constitutes a good example why modeling is important, especially when there are related observations. Current JWST observations find no atmospheres for the first planet *TRAPPIST-1b* (Ih et al., 2023), however contamination of the spectrum from the star can not be ruled out, leaving room for detection of potential atmospheres (Lim et al., 2023). However using atmospheric modeling, and taking into account other factors like the planet's host star, (Van Looveren et al., 2024) finds that any kind of atmosphere is unlikely for the *TRAPPIST-1* planets, whether contamination of the transit spectrum occurs or not.

Exoplanet observations give us either transit or emission spectra with which model results can be compared. The most common method using these spectra is a process called forward modeling. Forward modeling refers to the process of using (assumed or simulated) stellar, planetary and atmospheric properties as an input to calculate how the resulting transit spectra would look like. To do this, forward modeling often includes radiative transfer modeling. Radiative transfer modeling is also needed to translate the input parameters (such as atmospheric absorbers, densities and crosssections) into a synthetic transit spectrum. Examples of forward modeling including radiative transfer modeling are petitRADTRANS (Mollière et al., 2019) and Kompot (Johnstone et al., 2018) combined with KompotSpec, which is also covered in Chapter 3. On the other hand inverse modelling is also possible, where the previously listed input parameters are now calculated from an observed transit spectrum. An example of this is TauREx (Waldmann et al., 2015) which is currently being used to interpret JWST transit spectra.

Both petitRADTRANS and TauREx account for radiative transfer. To do this they split the atmosphere into pressure-temperature grids, which determine the absorption crosssections of atmospheric reactions and constituents. Combined with the associated densities, optical depths, transit depths and therefore the transit spectrum are calculated. Both codes make heavy use of Markov Chain Monte Carlo (MCMC) to retrieve the spectra / the associated atmospheric information. Both codes also make use of several data sources such as HITRAN/HITEMP (two separate databases used in conjunction) and ExoMol for opacities, crosssections and pressure broadening coefficients. For discussion of other retrieval codes and comparisons consult MacDonald and Batalha (2023).

1.3.2. Chemical kinetics

Chemical kinetics model in general concern themselves with the study of chemical reaction rates. The equations governing these reaction rates are often not solvable analytically, and are instead evaluated using numerical methods to solve for an atmospheric structure, which can then be further processed into a synthetic transit spectrum.

Chemical equilibrium codes

Chemical Equilibrium (CE) describes a state, where the concentrations of reactants in a system (such as an atmosphere) do not change in time. CE situations typically occur when photochemistry can be neglected Stock et al. (2018) and as such do not deal with radiative transfer. CE models have been used to calculate chemical compositions of stellar atmospheres (Tsuji, 1973), brown dwarfs (Helling et al., 2008a,b) and of course exoplanetary atmospheres (Kataria et al., 2014; Morley et al., 2015). These CE codes generally work by minimizing Gibbs free energy via numerical methods, examples for such codes include FastChem (Stock et al., 2018) and GGChem (Woitke et al., 2018).

Photochemical codes

Studies such as Morley et al. (2017) have shown that many exoplanets are in thermochemical disequilibrium, meaning CE assumptions are not valid for every object. As such, in addition to the calculations for CE codes, photochemical codes such as VULCAN (Tsai et al., 2021) and FRECKLL (Al-Refaie et al., 2024) need to solve continuity and diffusion equations and also incorporate radiative transfer into their calculations. The chemistry model of the Kompot code also falls into this category (Johnstone et al., 2018).

Three-dimensional GCM codes

3D General Circulation Model (GCM) codes, originally developed for understanding of the Earth's atmosphere, model circulation within a planetary atmosphere by dividing the entire atmosphere into cells, often with longitude, latitude and height in the atmosphere as coordinates (hence 3-dimensional). GCMs then solve the Navier-Stokes equations for a rotating sphere on this grid. Many terms are included in the Navier-Stokes equation, including radiative transfer, surface processes, chemistry, evaporation, precipitation and others (Wolf et al., 2019). By including surface interactions, GCMs such as ROCKE-3D (Way et al., 2017) can not only estimate surface temperatures, but also albedos and possible greenhouse effects for an ensemble of exoplanets (Del Genio et al., 2019). GCMs are also expected to describe tidally locked exoplanets well, due to incorporation of the atmospheric dynamics at their day-night terminator Wolf et al. (2019).

1.4. Motivation behind this work

Atmospheric characterization has come a long way since the first observations in the era of HST and Spitzer. Decades later JWST now provides unprecedented wavelength coverage with highly detailed data in the infrared spectrum, which lead to the first detection of photochemistry in an exoplanetary atmosphere (Tsai et al., 2023). Without these atmospheric models it seems difficult to impossible to interpret JWST data correctly. One of these is the one-dimensional atmospheric model Kompot detailed in Chapter 2. This work originated from the fact that the Kompot model provides simulations of exoplanet atmospheres and the associated thermal and very detailed chemical profile, including Jeans escape rates Johnstone et al. (2018). However it lacks the radiative transfer code necessary to produce atmospheric transmission spectra and compare its results to other forward modeling codes. With that in mind, a radiative transfer module KompotSpec was developed, capable of producing synthetic transit spectra in the ultraviolet and infrared ranges. KompotSpec was applied to Kompot simulations of Earth and Titan, and their synthetic transit spectra are compared to observations.

1.4.1. Structure of this work

This thesis is organized in a general introduction to exoplanets and atmospheres in Chapter 1, descriptions of the used atmospheric model Kompot in Chapter 2, the developed code KompotSpec in Chapter 3 and the results of Earth and Titan simulations as well as validation data in Chapter 4. Finally, final remarks and future improvements are presented in Chapter 5.

2. Model Description

2.1. Kompot model

The Kompot code (Johnstone et al., 2018) simulates a cloud-less exoplanetary atmosphere and the influence of its host star on its atmospheric processes. Those being heating of the atmosphere, ionization of atmospheric neutral species, photochemistry induced by the star's radiation and loss of atmospheric contents to space. Figure 2.1 illustrates the basic geometry of a Kompot simulation. The planet (black in the bottom right of Figure 2.1) is encircled by the lower and upper atmosphere. The lower boundary can be adjusted but is recommended to be kept above the cloud level, as Kompot does not simulate clouds. The exobase marks the outer limit of the atmosphere and is the upper boundary of the simulation domain. The Kompot code only simulates the upper atmosphere of the considered planets (Kompot models used in Chapter 4 use pressure ranges from $0.49 \cdot 10^{-5}$ bar to vacuum for Titan, and 1 bar to vacuum for Earth). The upper atmosphere is divided into cells of increasing size with altitude for efficiency. Realistic input parameters then need to be assumed to ensure simulation convergence. Atmospheric evolution is modeled using timesteps of length Δt, with XUV, IR, and nonthermal electron spectra calculated per cell (Johnstone et al., 2018). Hydrodynamics, chemistry, diffusion, heating/cooling, energy exchange, and conduction are simulated, though not all processes are recalculated at every timestep to balance accuracy and computation time. Various solvers address the equation systems of each process. The simulation proceeds until a steady-state atmosphere is achieved, with chemical evolution originally modeled via a custom network of around 500 reactions (Johnstone et al., 2018) at first release. Since then the chemical network has grown to more than 700 reactions, crucially supporting CH_4 necessary for Titan simulations in Chapter 4 (Boro Saikia, prep). A key input parameter of Kompot is the stellar XUV spectrum (refered to as the input spectrum). Additionally, input parameters such as initial atmospheric composition, height of lower simulation boundary as well as planetary mass and distance to its host star are necessary.

As seen in Figure 2.1, the simulation domain is a one-dimensional height column instead of simulating this layer of the atmosphere all the way around the planet. The latter would be desirable, since planetary atmospheres are generally not homogeneous (given effects such as tidal locking or day/night sides of the planet). This would however significantly increase computation time[1]. Also visible in Figure 2.1: the simulation domain is not at the substellar point, but instead at an angle relative to the incoming radiation of

[1]This one-dimensional Kompot version is routinely being run on the Vienna Scientific Cluster (VSC) with execution times of hours/days).

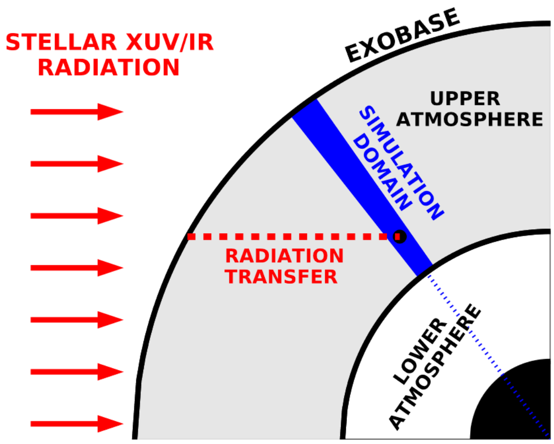

Figure 2.1.: Sketch of the Kompot computational domain, Source: Johnstone (2018)

the host star. This zenith angle is manually set and can be varied for probing different regions of the atmosphere. There are various possibilities for choosing this angle (as seen in Figure 2.2). While the angle can be set freely, a value of 66° degrees is typical for Earth studies (represented in Red in Figure 2.2. This is because for studies of the Earth, this value produces a good average representation of Earth's atmosphere across different latitudes (Johnstone et al., 2018, 2021b). This angle is likely to be less applicable to planetary atmospheres other than Earth's. The anti-substellar point, as any point on the far hemisphere of the planet in relation to the star, is not a sensible choice for zenith angle.

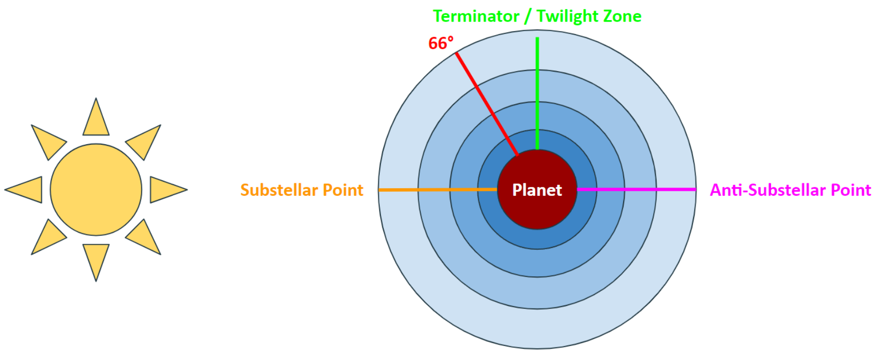

Figure 2.2.: Illustration of zenith angles and most-used Kompot value in Red

Kompot has been validated against solar system planets such as Mars (Amerstorfer et al., 2019) and Earth (Johnstone et al., 2019). For Earth, Kompot studies suggest that Earth had up to 40% CO_2 in its atmosphere approximately 3.8 Gyrs ago, thereby indirectly constraining the Sun's XUV evolution during its lifetime. Currently, with the inclusion of CH_4 chemistry into Kompot it is also being tested against Titan data (Boro Saikia, prep), some preliminary data being used for the plots in Chapter 4. Kompot studies around habitability of exoplanets are also viable, such as Van Looveren et al. (2024) investigating the *TRAPPIST-1* system and strongly suggesting that a terrestrial atmosphere with present-day irradiation of the M-dwarf *TRAPPIST-1* would be stripped within a few hundred Myrs.

2.1.1. Simulated processes

Kompot calculates the thermo-chemical structure of planetary atmospheres. For chemistry, the code takes into account around 700 different chemical/photochemical reactions (Boro Saikia, prep). These include light elements such as H and He, but also metals such as C, N, O, Cl and Ar and combinations as well as their ions. Eddy and molecular diffusion as well as advection are also modeled in the Kompot code. For the thermal structure of the atmosphere, a number of processes are modeled in Kompot. For example stellar X-ray, ultraviolet and infrared radiation (which is provided to Kompot in the input stellar spectrum) and its effects on the atmospheric expansion/contraction. Heating from electron collisions with non-thermal photoelectrons and heating from exothermic reactions is also modeled. Cooling of the atmosphere from infrared emission of atmospheric species is also included, as are thermal conduction and energy exchange between the electron gas, ions and neutrals.

The atmospheric expansion/contraction is modelled by continuously recalculating the exobase (the upper boundary of the simulation). This is done by equating for the mean free path λ_{mfp} (Equation 2.1) and scale height H (Equation 2.2). The height at which λ_{mfp} equals H is considered the upper simulation boundary, the exobase. Where σ is a simplified collision cross section, n is number density, k_B is the Boltzmann constant, m is the average molecular mass, and g is the gravitational acceleration at the exobase (Van Looveren et al., 2024).

$$\lambda_{mfp} = \frac{1}{\sigma\, n} \tag{2.1}$$

$$H = \frac{k_B\, T}{m\, g} \tag{2.2}$$

2.1.2. Free parameters & assumptions

Kompot's model makes several assumptions, such as equal bulk advection speeds for gasses (with different diffusion speeds for each species). Additionally neutrals, ions and electrons each have independent temperatures and temperature evolutions. Finally quasineutrality, meaning equal electron and ion density everywhere, is assumed (Johnstone et al., 2018). A significant strength of the Kompot code is that no free parameters, such as the heating efficiency, have to be assumed (Johnstone et al., 2021b). Heating efficiency is defined by the ratio of energy converted into heating of the atmosphere divided by the total energy input of the atmosphere. Its values range from zero to one, however the value of assumed heating efficiency can vary drastically (for a summary of authors and their values consider Ionov and Shematovich (2015)). As such elimination of such a parameter from the model is highly desirable.

After the initial simulation parameters are set, the code starts applying the aforementioned processes sequentially iteration by iteration. If a stable, self-consistent model of the upper atmosphere is reached the simulation terminates successfully. Included in the simulation outputs are reaction rates, chemical makeup as well as thermal structure of the atmosphere (Van Looveren et al., 2024). The chemical makeup is by far the most relevant output for this work, as this directly influences abundances of elements in the atmosphere, and the measurable absorption in the transit spectrum. While thermal structure is also of interest for simulations, planetary atmospheric emission in the infrared has not been implemented in this work.

2.2. Limitations

2.2.1. One-dimensional simulation

As mentioned, Kompot's simulations are one-dimensional in nature and at a specific angle/region of the atmosphere. This means Kompot can only reproduce average atmospheric composition for an exoplanetary atmosphere (since the zenith angle is an approximation of an average atmosphere). If study of specific regions of the planet, such as atmospheric composition directly at the substellar point (in orange in Figure 2.2) or the terminator / twilight zone (in green in Figure 2.2) is of interest, Kompot's results need to be verified. Especially since three-dimensional effects, which will be present in these regions, can not be considered by Kompot's model. This warrants further study in the future, especially since chemical properties and the transit spectrum would also change depending on the simulated region.

2.2.2. No clouds / hazes considered

Formation of clouds or hazes is not modeled in Kompot. Which can be problematic, because clouds/hazes or lack thereof can significantly interfere with transit spectra (especially synthetic ones explored in the later parts of this work) in a number of ways. Not simulating them / considering this fact in analysis of results could lead to misinterpretation of the measured planetary atmospheres. Kompot avoids this by setting the lower boundary of its simulation above the cloud layer, thereby forgoing this problem. This also limits Kompot and this work to dealing with cloudless atmospheres. Clouds/hazes typically influence observed transit spectra by flattening them, meaning same transit depth across all wavelengths λ (Knutson et al., 2014). Alternatively, slopes (with larger transit depths at smaller wavelengths λ) can also appear in the observed spectra (Jordán et al., 2013; Lecavelier des Etangs et al., 2008).

3. KompotSpec

KompotSpec is a model based upon Kompot's atmospheric simulations. KompotSpec takes Kompot's simulation domain and results, transforms them from a one-dimensional geometry into one suited for calculating transit spectroscopy and performs wavelength-dependent optical depth calculations for the different heights and absorbing species within the atmosphere. Based upon these calculations, synthetic transit spectra for the simulated atmosphere in total and each of its molecular components are created. As Kompot provides the necessary data in the XUV/UV, KompotSpec can be run in this wavelength range without further data. Since the infrared is however much more relevant in current transit spectroscopy, KompotSpec can also model transit spectroscopy in the infrared by downloading additional crosssection data from the ExoMolOP project (Chubb et al., 2021). This enables comparison of Kompot-based simulations with potential observations from instruments such as JWST.

KompotSpec fills a gap, making Kompot's results comparable to other codes dealing with radiative transfer, such as petitRADTRANS or TauREx. Very much alike petitRADTRANS it also makes use of chemical models in disequilibrium (Mollière et al., 2019) when modeling an atmosphere with presumably significant photochemistry. The retrieval code TauREx, although doing the inverse of KompotSpec (retrieving atmospheric properties from an observed spectrum), supports only equilibrium chemistry in its current version 3 (Al-Refaie et al., 2021). As such the Kompot/KompotSpec combination uses a promising chemical model which has not been previously used for forward modeling. Another similarity between Kompot/KompotSpec and petitRADTRANS is that both do not account for scattering in the atmosphere and therefore cannot account for clouds. A slight advantage for Kompot/KompotSpec is that its simulation domain is situated above cloud height, negating a potential pitfall of the code. In summary, Kompot/KompotSpec fits well into the existing ecosystem of atmosphere modeling codes and, despite its performance not yet being as optimized as its competitors, brings a new way to characterize exoplanetary atmospheres using transit observations.

3.1. Model setup

One drawback of Kompot is the fact that just a one-dimensional slice of the atmosphere is simulated at a certain zenith angle. This becomes a problem when one wants to model transiting light beams, since light rays passing close to the surface would only experience absorption of the bottom-most cell in the left side of Figure 3.1. Instead such light rays have to pass through higher atmospheric layers in order to reach the lower atmospheric layers, its absorption being altered by each layer on the right side of Figure 3.1 . As such, information about the atmospheric composition at one specific height column in the atmosphere is insufficient.

To overcome this problem, assumptions are made about the atmospheric composition. The assumption being that the atmospheric composition of the one-dimensional slice by Kompot is uniformly adopted for the entire atmosphere of the planet. Thereby effectively extending the one-dimensional coverage across the whole planet, as is illustrated in Figure 3.1. More advanced ideas such as interpolating the one-dimensional slice / using weather models to vary the atmosphere based on zenith angle were determined to be left for future improvements.

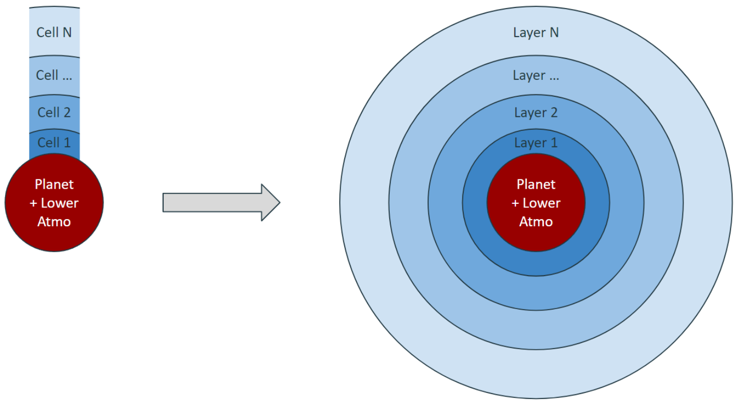

Figure 3.1.: Left: Kompot simulation domain and associated cells (including height, P-T, density and species data), Right: KompotSpec simulation domain with Kompot cells expanded to circular layers (with same height, P-T, density and species data)

In terms of radiative transfer, equation 3.5 in Subsection 3.2.1 assumed the source function to be zero. As a consequence, this means that both scattering in the atmosphere as well as emission (including thermal reemission) are not considered during the radiative transfer process. As a result, KompotSpec does not simulate scattering or reemission processes. While both of these are without a doubt common in many atmospheres, this can be added in future iterations of the code.

As a result, unlike other modeling codes (mentioned in Subsection 1.3.1), KompotSpec can not be used for emission spectroscopy. Losses by light scattering off the line-of-sight are not taken into account. And neither is when energized molecules re-radiate their stored energy in the infrared wavelengths. Both of which are processes that have the potential to impact the resulting synthetic transit spectrum.

3.2. Radiative transfer in KompotSpec

Understanding of the radiative transfer equations is essential to understand the inner workings of any code dealing with radiative transfer, and the same goes for this work. The following equations and figures aim to illustrate the mathematical background, its simplifications and transit geometry used in this work.

3.2.1. Derivations of radiative transfer equations

The first quantity that we will introduce is the optical depth τ_ν. The higher the optical depth the more opaque a medium is to electromagnetic radiation, whereas optical depths approaching zero describe nearly transparent mediums. In equation 3.1 $\kappa_\nu = \kappa_a + \kappa_s$ is the extinction coefficient (reflecting the sum of the absorption and the scattering coefficient), ρ the mass density of the medium, both of which are integrated along a chosen path s.

$$\tau_\nu = \int \kappa_\nu \, \rho \, ds \tag{3.1}$$

The influence of not just extinction, but also emission can be expressed by the source function S_ν in equation 3.2. j_ν herein is the emission coefficient,

$$S_\nu = \frac{j_\nu}{\kappa_\nu} \tag{3.2}$$

Taking the above equations into account we can write down the radiative transfer equation 3.3, which describes how radiation is impacted when passing through a medium. The introduced terms I_ν and $\frac{dI_\nu}{d\tau}$ are the wavelength-dependent intensity of the light, as well as the decrease of intensity for a given optical depth.

$$\frac{d\,I_\nu}{d\,\tau_\nu} = -I_\nu + S_\nu \tag{3.3}$$

The source function S_ν is rarely analytical and often has to be assumed / approximated numerically. This is because the scattering of light is generally not the same in all directions. Therefore the source function would include influx of light scattered into the beam from elsewhere, leading to high complexity. Equation 3.3 becomes solvable for constant source functions S_ν, meaning constant ratios of emission to extinction. Since neither scattering nor emission is modeled in this work, we adopted $S_\nu = 0$ which, after some simplification in equation 3.4 leads to equation 3.5. This equation is known as Lambert's, Bouguer's or Beer's law.

$$\begin{aligned} \frac{d\,I_\nu}{d\,\tau_\nu} &= -I_\nu \\ \int_0^{\tau_\nu} \frac{1}{I_\nu}\;d\,I_\nu &= -\int_0^{\tau_\nu} 1\;\,d\,\tau'_\nu \\ ln\,I_\nu \Big|_0^{\tau_\nu} &= -\tau'_\nu \Big|_0^{\tau_\nu} \\ \frac{ln\,I_\nu(\tau_\nu)}{ln\,I_\nu(0)} &= -\tau_\nu \end{aligned} \tag{3.4}$$

Equation 3.5 now lets us describe how absorption crosssections κ_ν and densities ρ of materials attenuate the light intensity I_ν (for example from a stellar input spectrum). These are all known quantities, densities ρ of atmospheric species being sourced from Kompot's simulated atmospheric data, and crosssections κ_ν fetched from different sources depending whether a transit spectrum in the UV or IR spectrum is desired (further described in Section 3.3). Also note that in subsection 3.4.6 we do not actually end up using the I_ν terms, since transit spectra can be calculated independent of the stellar irradiation I_ν. This excerpt instead serves as justification for using the $e^{-\tau_\nu}$ term from equation 3.5 in our transit spectra calculations, and showing it follows directly from the radiative transfer equation.

$$I_\nu(\tau_\nu) = I_\nu(0)\,e^{-\tau_\nu} = I_\nu(0)\,e^{-\int \kappa_\nu\,\rho\,ds} \tag{3.5}$$

3.2.2. Radiative transfer geometry in KompotSpec

A single light ray (from the host star) can be seen transiting through the atmosphere tangentially and exiting the atmosphere on the other side in Figure 3.2. This plot shows the light ray passing through different layers[1] of the atmosphere, from the top of the atmosphere to the bottom of the considered atmosphere. Each layer of the atmosphere contains different atmospheric species with different mass densities ρ. Each of these species also have different properties for absorption processes (also for scattering and emission processes, though not considered in KompotSpec), which are themselves wavelength-dependent.

To calculate the optical depths τ for each layer of the atmosphere via equation 3.1, not only are mass densities ρ and extinction coefficients κ_ν (also called absorption coefficients) needed, but also the path s the considered ray spends within each layer. A graphical representation of this can be found in Figure 3.3. While in the figure the layers are quite close in size, in the case of Kompot/KompotSpec, the upper layers are multiple orders of

[1] The term "layer" is henceforth used, since an atmosphere in Kompot is divided in discrete "cells". It is also easier to visualize. For a continuous atmospheric profile it would make sense to instead use "height"

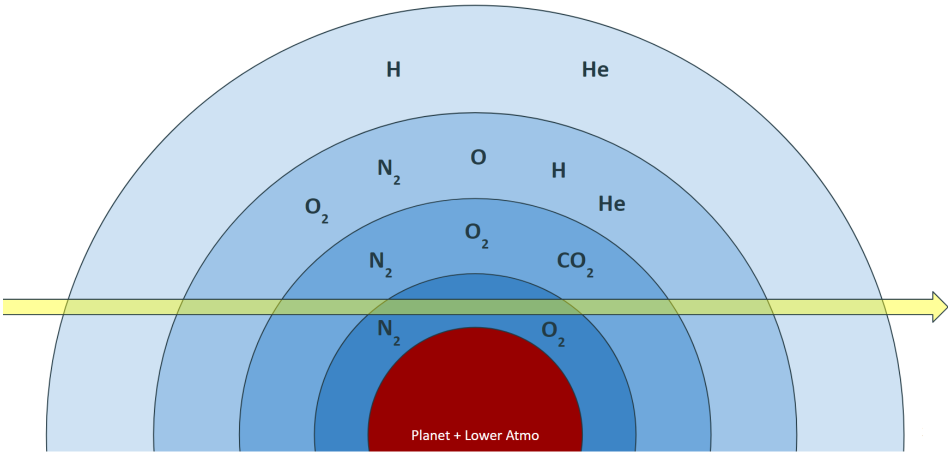

Figure 3.2.: Sketch of a single light ray from host star transiting through planetary atmosphere (Earth-like) with different constituent species and densities

magnitude bigger than the bottom ones. However, the light ray in Figure 3.3 is drawn very close to the lower boundary of the considered atmosphere. When actually measuring a transiting exoplanet / the atmosphere of said planet we measure a convolution of light rays. So both rays transiting deep in the atmosphere, as well as higher "grazing" rays are measured simultaneously. In order to properly sample a simulated atmosphere the same way it is observed, more light rays at different positions/heights in the atmosphere are introduced. The resulting geometry is sketched out in Figure 3.4.

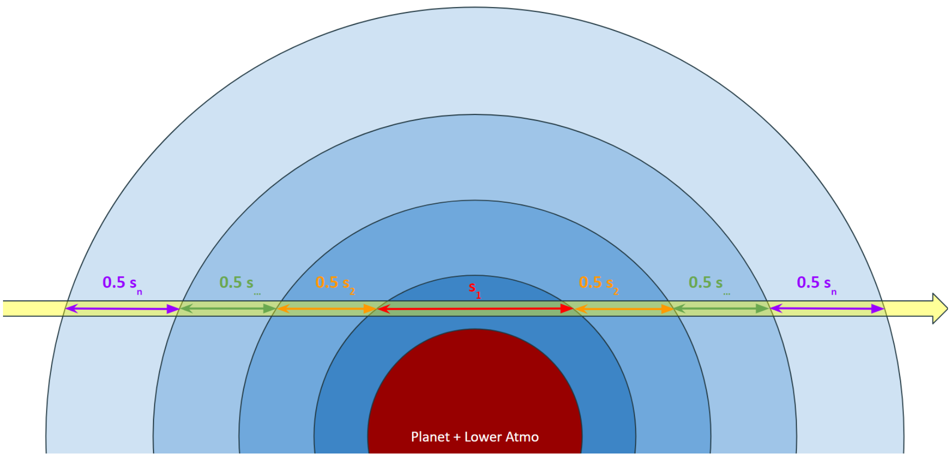

Figure 3.3.: Sketch of a single light ray from host star transiting through planetary atmosphere (Earth-like) with different path lengths within each layer

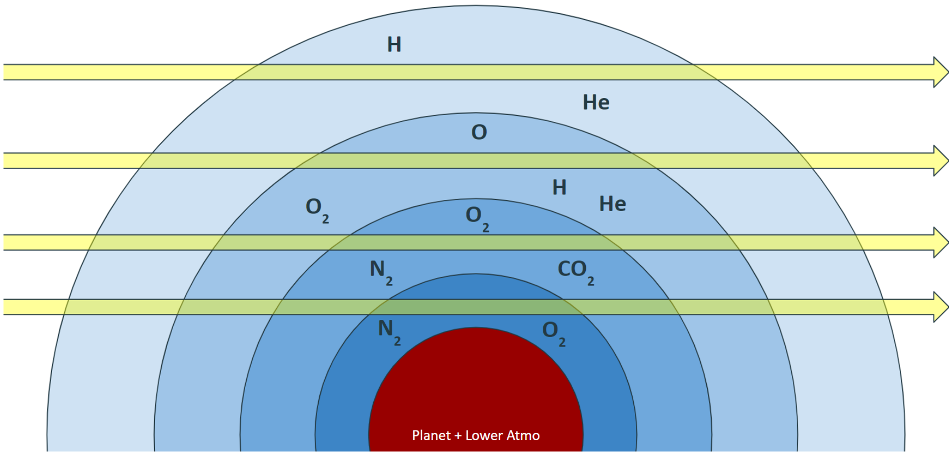

Figure 3.4.: Sketch of multiple light rays from host star transiting through planetary atmosphere (Earth-like) at different heights

3.3. Absorption crosssections

KompotSpec can work in a UV mode, where it uses the given UV crosssections and calculates transit spectra in the same range. Alternatively KompotSpec can run in an infrared mode where an infrared transmission spectrum is generated, which requires infrared crosssections. If both UV and infrared transit spectra are desired, they need to be done in separate KompotSpec runs. Both of the crosssection modes have different data sources, which are outlined below.

3.3.1. Ultraviolet crosssections - Kompot

Since Kompot performs radiative transfer of the incoming stellar radiation in the XUV, the crosssections available are in the UV wavelengths. As such these same crosssections are then reused by KompotSpec to calculate the transit spectrum in the UV range. The sources for the crosssections for the simulated species can be found in Johnstone et al. (2018).

3.3.2. Infrared crosssections - ExoMolOP

Alternatively KompotSpec can run in an infrared mode where an infrared transmission spectrum is generated, which requires infrared crosssections. The infrared crosssections are sourced from the ExoMolOP database (Chubb et al., 2021). ExoMolOP is in itself a combination of data from ExoMol, HITEMP, MoLLIST, HITRAN and NIST. The compiled data provides high-resolution crosssections (spectral resolution R of 15000) for more than 80 species between 300 and 50000 nm. Pressure-broadening coefficients, among other data, are also provided by the database. The data comes pre-packaged to work seamlessly with popular atmospheric modeling codes. KompotSpec makes use of ExoMolOP data which is available in the format used by the atmospheric retrieval code TauREx (Chubb et al., 2021) (TauREx's format being chosen since it required minimal adaption for use with KompotSpec). Each absorbing species is stored in a separate file which contains crosssection data for different pressure and temperature levels. The ExoMolOP pressure-temperature grid (P-T grid) contains 22 pressure points from 0.01 mbar to 100 bar, and 27 temperature points from 300 to 3400 K respectively.

3.4. KompotSpec Workflow

3.4.1. Setup & execution

In the KompotSpec settings file the parameters for the simulation are set. For an overview and quick explanation of configurable parameters consult Table B.1. When initial parameters are set, the simulation is ready to be started. Initially the needed external libraries are loaded, and folders for storing the outputs are created. The input files used in the simulation (containing the structure, P-T data of the atmosphere and IR/UV crosssections) are copied into the output folder. As are the used KompotSpec code files to be able to reproduce the simulation easily.

3.4.2. Crosssection loading & plotting

KompotSpec in its infrared mode first calculates the closest ExoMolOP P-T grid point for each atmospheric layer. Only the needed (P-T dependent) crosssection tables atmosphere are then loaded into memory. For layers without pressure/temperature data provided in Kompot, pressure/temperature for the closest layer with such data is used. In the case of the UV mode (only one crosssection table) it ends up just using Kompot's provided UV crosssections instead.

With the loaded crosssection data, crosssection plots of each simulated absorber in KompotSpec are created. For the UV mode, a single crosssection profile is plotted for each absorber. In its infrared mode, all of the (simulation-relevant) P-T crosssection profiles are plotted for the absorbers.

3.4.3. Data sanitation & internal simulation parameters

The data sources (Kompot's atmospheric structure file and the crosssection tables) are re-organized. Columns are re-arranged into the same order, and incomplete datasets (e.g. where atmospheric densities are available, but crosssections are not) are dropped. The simulation aborts if column names and their order does not match after this process, since faulty indexing will otherwise produce wrong results.

Upper and lower simulation boundaries are set. The lower boundary for KompotSpec is the same one as the lowest cell in Kompot, whereas the upper boundary is instead the highest Kompot cell that has densities (layers above are not calculated as they are above the exobase). The spacing of the light rays (as in Figure 3.4) is also set. Currently the light rays are linearly spaced in between the lower and upper simulation boundary.

3.4.4. Path & area calculations for light rays

Prior to starting radiative transfer calculation, each light ray's path through each atmospheric layer is calculated as depicted in Figure 3.3. Additionally for each light ray, the area of the annulus between itself on the upper end and the light ray below on the bottom end is calculated. These are calculated since the rays will later be weighted, according to the crosssectional area of the atmosphere they are sampling. Figure 3.5 shows this weighting is needed for transit depth calculation, since higher rays sample much larger atmospheric regions (by crosssection area). To clarify, the view in Figure 3.5 is different from geometry's such as Figure 3.4. Figure 3.5 assumes the host star to be out of plane with the page, towards the reader. Whereas the previous plots like Figure 3.4 assumed the host star to be on the left side of the figure.

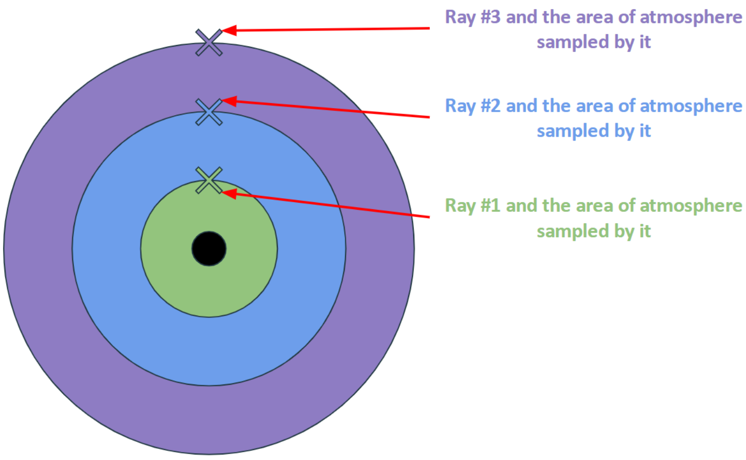

Figure 3.5.: KompotSpec light rays and regions of atmosphere sampled by them

3.4.5. Optical depth calculation & plotting light ray paths

For each light ray we iterate over all wavelengths and perform radiative transfer for this combination. The total optical depth of for the light ray/wavelength pair is given by equation 3.6.

$$\tau_{Ray} = \sum \tau_{Layer} \tag{3.6}$$

Optical depths τ_{Layer} have to then be calculated for each layer in equation 3.7, since the path s_{Layer} is different for each one. $\rho_{Absorber}$ is also dependent on the layer, but mainly on which absorbing species is considered. The absorption crosssection $\sigma_{Absorber}$ behaves the same way in the infrared mode, since layers with different P-T values have different crosssection tables for their absorbing species.

$$\tau_{Layer} = s_{Layer} \sum \sigma_{Absorber}\, \rho_{Absorber} \tag{3.7}$$

Additional plots are created by showing each atmospheric layer on the x-axis, and the distance each light ray covers within aforementioned layer. This is used to diagnose issues and find out which layers are probed by the simulated rays. Equally it shows which parts of the atmosphere are not probed by the simulation.

3.4.6. Transit spectrum generation

Transit spectra are now calculated with the calculated optical depths. For this, we use equation 3.8 (equation 7 from Mollière et al. (2019)) to convert calculated optical depths into "effective areas" of the atmosphere. "Effective area" is referring not to the physical area denoted by A, but to the area of a totally opaque medium which has the same amount of absorption. For example, even though an atmosphere has a very large crosssection area, it could have an effective area orders of magnitude smaller, depending on how transparent / how large the optical depth τ is in an atmosphere. To avoid confusion, we adopt that physical areas are denoted by the letter A, whereas effective areas are denoted by Θ.

$$\Theta_{Planet} = \; 2\pi \int_0^{R_{Planet}} r\; (1 - \exp(-\tau))\; dr \tag{3.8}$$

The use of "effective area of a planet" in Mollière et al. (2019) is misleading, as the nomenclature could imply that we are also integrating the planet's interior. However it clears that up by stating that the equivalent area of the atmosphere is instead integrated from the planetary surface up to R_{Planet} (includes atmospheric radius), resulting in equation 3.9.

$$\Theta_{Atmosphere} = \; 2\pi \int_{R_{Surface}}^{R_{Planet}} r\; (1 - \exp(-\tau))\; dr \tag{3.9}$$

Calculating the integral in equation 3.9 yields equation 3.10. Note that the term $[R^2_{Planet}\,\pi - R^2_{Surface}\,\pi]$ is just the area of the total atmosphere, or the area of a circular annulus with inner and outer Radius of $R_{Surface}$ and R_{Planet} respectively.

$$\Theta_{Atmosphere} = [R_{Planet}^2 \pi - R_{Surface}^2 \pi] \, (1 - \exp(-\tau)) \tag{3.10}$$

Since the regions sampled by each KompotSpec light ray are also circular annuli, we can calculate the equivalent area of such a region Θ_{Ray} in the same way, presented in equation 3.11. We replace $[R_{Planet}^2 \pi - R_{Surface}^2 \pi]$ by A_{Ray}, the area of the circular annulus between the height of the considered ray and the one below it (or the simulation boundary for the lowest ray). We also replace the generic τ by τ_{Ray}, which was calculated in equation 3.6.

$$\Theta_{Ray} = A_{Ray} \, (1 - \exp(-\tau_{Ray})) \tag{3.11}$$

With these definitions, we can calculate the total effective area of a simulated atmosphere Θ_{Total} as a simple sum of partial effective areas for each light ray in equation 3.12.

$$\Theta_{Total} = \sum \Theta_{Ray} \tag{3.12}$$

Finally, since effective and physical area have the same dimensions, we can modify the standard equation for transit depth δ to get equation 3.13.

$$\delta = \frac{R_{Planet}^2 \pi + \Theta_{Total}}{R_{Star}^2 \pi} = \frac{A_{Planet} + \Theta_{Total}}{A_{Star}} \tag{3.13}$$

These wavelength-dependent transit depths δ are calculated for each absorber individually, and then saved in an *.xlsx* file in native wavelength resolution for later use.

Rebinning & plotting

By executing the provided file it is possible to plot the transit spectra calculated during KompotSpec's simulation. For this purpose the *.xlsx* file is read, where the transit spectra are stored. The data is used to produce transit spectrum plots, both for each absorber separately as well as all absorbers combined into one plot (All of these use units of nm and ppm for the x-axis and y-axis respectively).

Further, plots can be customized by constraining the plotted x-wavelength range (in units of nm), since most of the time the native wavelength range is much too broad for readable plots. This feature was used to plot KompotSpec's results in Chapter 4, and compare them to validation data provided by Lustig-Yaeger et al. (2023) for Earth and Robinson et al. (2014) for Titan. Additionally, simple rebinning is possible, where n wavelength bins are rebinned into a single one. For this purpose, both wavelength and transit depth are averaged over the n bins.

4. Results

In this chapter we use the KompotSpec code on previously simulated Kompot atmospheres. Results are presented for simulated Earth and Titan atmospheres. After introducing KompotSpec's synthetic transit spectra, real transit spectra are used to compare our results to observational data. Comparison data for the Earth atmosphere is provided by Lustig-Yaeger et al. (2023), and by Robinson et al. (2014) for the Titan atmosphere. Finally, both spectra, their absorption features and the elements causing the features are compared.

4.1. Simulation results of an Earth-like atmosphere

With an Earth ($M = 1\,M_\oplus$ and $R = 1\,R_\oplus$) atmosphere simulated by Kompot (see Appendix D for atmospheric composition), and the KompotSpec parameters listed in Table 4.1 the synthetic transit spectra in Figure 4.1 and Figure 5.1 were simulated. Comparison data from Lustig-Yaeger et al. (2023) is provided in Figure 4.3.

4.1.1. KompotSpec Earth simulation

Parameter	**Value**
N_rays	20
RADIUS_PLANET [m]	6 378 000
RADIUS_STAR [m]	696 342 000
CROSSSECTION_MODE	ExoMol/IR
Simulated species crosssections	O_2, NO, H_2O, OH, CO, CO_2, OH^+, $H_2{}^+$, $H_3{}^+$, H_2O_2, NH, HeH^+, H_3O^+, N_2O, HNO_3, SO, SO_2, CS, OCS, H_2S, SO_3, CN, CH_4, CH_3, HCN, C_2H_2, CH, C_2H_4, C_2

Table 4.1.: KompotSpec parameters for Earth simulation

KompotSpec's resulting transit spectrum is shown in Figure 4.1, with the KompotSpec parameters in Table 4.1 used to create it. The CO_2 absorption features found at 2.6, 4.3 and 15 μm are all present. O_3, which would be expected in an Earth atmosphere, is missing, however this is due to the unavailability of O_3 crosssections in ExoMolOP, which lead to it not being included in the simulation. H_2O, the third promiment absorber in the comparison transit spectrum, also appears prominently in KompotSpec's transit spectrum from around 4.5 to 7.5 μm and again centered at around 2.7 μm. KompotSpec also introduces minor NO features at 4.6 to 4.8 μm and at around 8 μm.

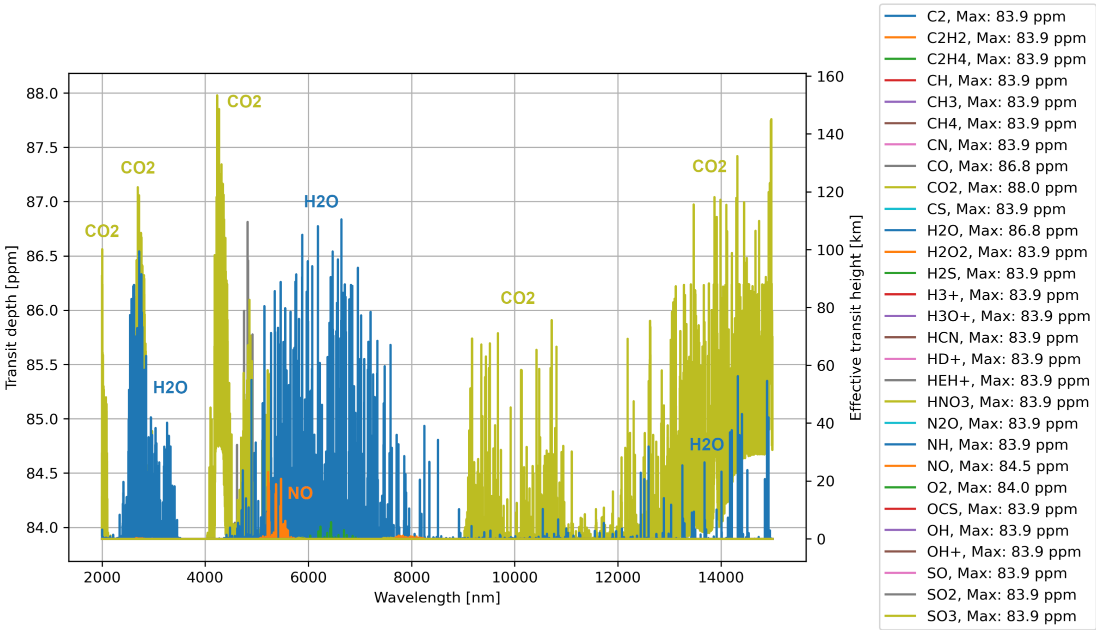

Figure 4.1.: Individual transit spectra of individual absorber contributions for Earth and maximum transit depth per absorber (No rebinning)

4.1.2. Comparison data

Lustig-Yaeger et al. (2023) use a transmission spectrum of Earth to retrieve its atmospheric constituents. The transmission spectrum was provided by Macdonald and Cowan (2019), with data from the Atmospheric Chemistry Experiment Fourier Transform Spectrometer (ACE-FTS) instrument of Scientific Satellite (SCISAT) (Bernath et al., 2005; Hughes et al., 2014; Boone and Bernath, 2019). Expecting possible usecases with JWST, they used an atmospheric model to extract properties from the observed transmission spectrum. The underlying atmosphere, both its mixing ratios and it P-T profile can be seen in Figure 4.2. Assumptions used to initialize the retrieval included a mean molecular weight of 29 g/mol, fixed surface pressure of 1 bar, planetary radius and mass of $R_\oplus$ and $M_\oplus$ respectively. Stellar parameters were set at a radius of $R_\odot$ and a distance of 1 AU.

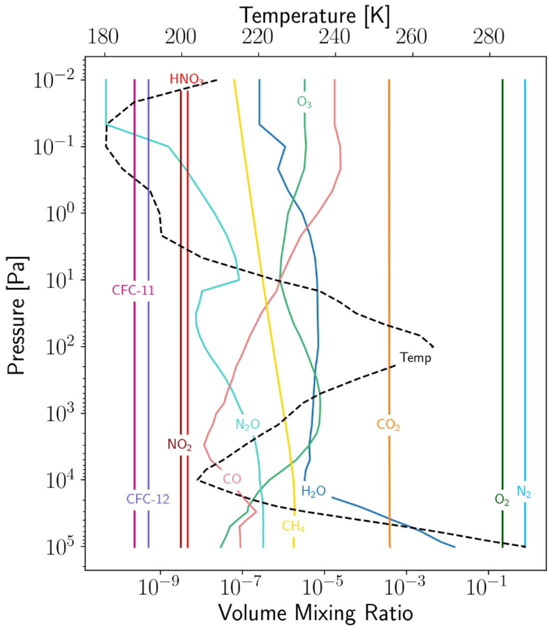

Figure 4.2.: Atmospheric model of Earth used to run forward models; Dashed black line: P-T profile of the atmosphere, Source: Lustig-Yaeger et al. (2023)

The observed transit spectrum in Figure 4.3 with overlaid absorber contributions will be used as comparison data for our own Earth simulations using KompotSpec. A wide variety of different absorbers can be seen in the transit spectrum with the retrieved atmospheric constituents. Chief among them are the three major absorbers CO_2, H_2O and O_3. Significant CO_2 absorption features can be found centered at 2.6, 4.3 and 15 μm (for the latter feature only the left flank is visible in Figure 4.3). O_3 has a broad absorption windows from around 8.5 to 10.5 μm, while H_2O has several broad but smaller absorption windows.

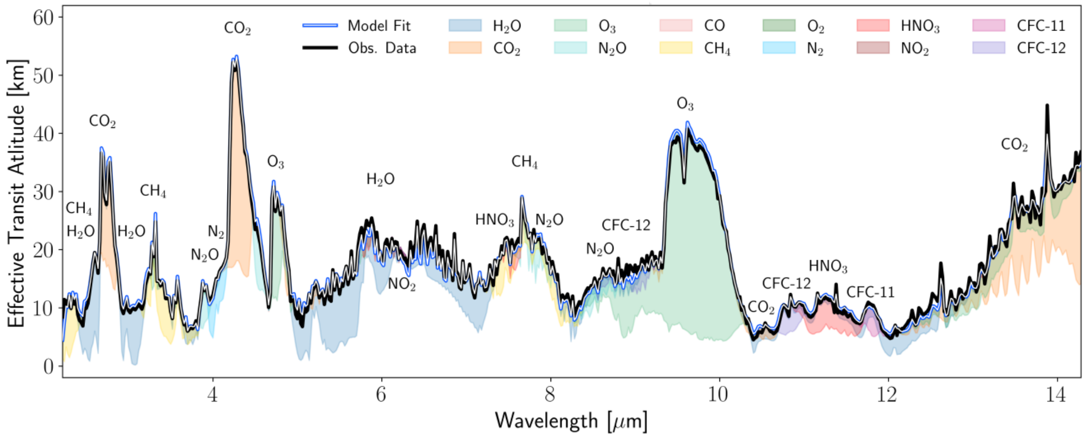

Figure 4.3.: Transit spectra of Earth with absorption by individual atmospheric species, Source: Lustig-Yaeger et al. (2023)

4.2. Simulation results of a Titan-like atmosphere

With a Titan ($M = 1\,M_{Titan}$ and $R = 1\,R_{Titan}$) atmosphere simulated by Kompot (see Appendix E for atmospheric composition), and the KompotSpec parameters listed in Table 4.2 the synthetic transit spectra in Figure 4.4 and Figure 5.2 were simulated. Comparison data from Robinson et al. (2014) is provided in Figure 4.5.

4.2.1. KompotSpec Titan simulation

Parameter	**Value**
N_rays	20
$RADIUS\_PLANET$ [m]	2 574 700
$RADIUS\_STAR$ [m]	696 342 000
$CROSSSECTION\_MODE$	ExoMol/IR
Simulated species crosssections	C_2H_2, C_2H_4, CH_4, CO, CO_2, H_2O, H_2O_2, H_2S, HCN, HNO_3, N_2O, NO, OCS, SO, SO_2

Table 4.2.: KompotSpec parameters for Titan simulation

KompotSpec's resulting transit spectrum is shown in Figure 4.4, with the KompotSpec parameters in Table 4.2 used to create it. We first find a flat continuum, and by further inspecting KompotSpec's results we find that major CH_4 peaks at 1.2, 1.4, 1.7, 2.3 and 3.3 μm are present. C_2H_2 surprisingly is not found at 3.1 μm, despite its crosssections being used in the simulation. CO at 4.6 μm also does not show up on the transit spectrum, despite also featuring in the simulation. The lack of C_2H_2 and CO features is caused by the low number densities of these molecules in the simulated Kompot atmosphere. The C-H stretching mode of aliphatic hydrocarbon chains at 3.4 μm is also not present in the spectrum, however unsurprisingly so, since it was not considered in the simulation. Finally KompotSpec predicts some absorption including significant H_2O features at 1.4, 1.9 and between 2.5 and 3.0 μm. Additionally, a strong HCN absorption is found at 3.05 μm and some minor C_2H_4 features at 3.2 - 3.3 μm, being overshadowed by the much more prominent CH_4 features.

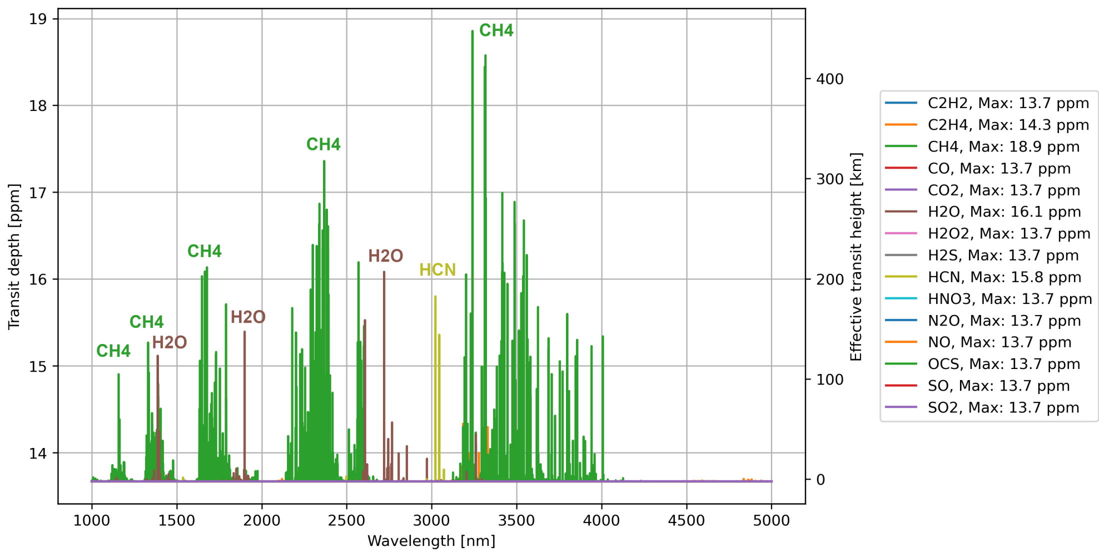

Figure 4.4.: Individual transit spectra of individual absorber contributions for Titan and maximum transit depth per absorber (No rebinning)

4.2.2. Comparison data

Robinson et al. (2014) uses solar occcultation data of Titan, taken by Cassini's Visual and Infrared Mapping Spectrometer (VIMS), to explore how hazes and clouds impact transit spectra. In this work however, we compare our KompotSpec simulation results with the resulting transit from Robinson et al. (2014). The wavelength range covered is between 0.88 and 5 μm with a wavelength resolution of 12 to 18 nm. Out of ten total measured transit, only four could be used due to problems with pointing stability and parasitic light (Robinson et al., 2014). These passes and their transit spectra are pictured in Figure 4.5, with additional information concerning which absorber is causing each peak in the spectrum, which will be compared to KompotSpec's effective transit heights. Remarkably, the continuum is sloped and wavelength dependent, which Robinson et al. (2014) attributes to hazes in the upper atmosphere of Titan. CH_4 clouds are thought not to affect the spectra, since they are typically found below 30 km (Rannou et al., 2006).

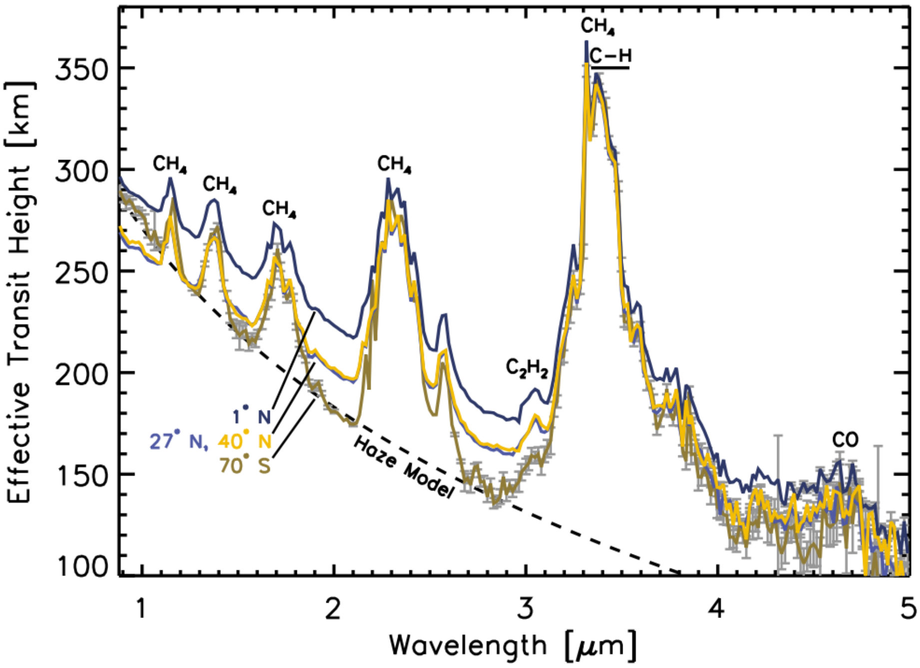

Figure 4.5.: Transit spectra of Titan, each line is a separate transit measurement during a flyby of Cassini (at different planetary latitudes), Source: Robinson et al. (2014)

Figure 4.5 also incorporates a model simulating high altitude hazes in Titan's atmosphere into their transit spectra. The key assumption is that the wavelength-dependent absorption crosssection of the hazes σ_λ is related to wavelength λ via the simple power law $\sigma_\lambda \propto \lambda^\beta$ (β being a free parameter). The model in Figure 4.5 is achieved using $\beta = -1.9 \pm 0.2$, a slope incompatible with pure rayleigh scattering at $\beta = -4$. This difference is thought to be due to the complexities in light scattering, caused by the high altitude hazes at a modeled scale height $H_a = 55 \pm 8$ km.

Titan's transit spectrum from Robinson et al. (2014) in the considered wavelength range is clearly dominated by CH_4, it making up the five major peaks in the spectrum in Figure 4.5 (at 1.2, 1.4, 1.7, 2.3 and 3.3 μm). Minor peaks are also caused by C_2H_2 at 3.1 μm , the C-H stretching mode of aliphatic hydrocarbon chains at 3.4 μm, partly obscured by the methane feature, and CO at 4.6 μm (Bellucci et al., 2009; Maltagliati et al., 2015).

5. Discussion

5.1. KompotSpec Earth simulation

Figure 5.1 combines the individual absorber effective transit heights into one spectrum, making the results from KompotSpec comparable to the comparison data in Figure 4.3. When reviewing the y-axis, especially the effective transit height in km, it quickly becomes apparent that those differ significantly. Also, the relative heights of e.g. the CO_2 feature at 4.3 μm and the H_2O feature from 4.5 to 7.5 μm are off, them being of similar magnitude. Compare for example KompotSpec's effective transit heights of around 140 km and around 100 km for the CO_2 and H_2O feature respectively, to the comparison data with around 55 km and around 25 km for the CO_2 and H_2O feature respectively. It seems that some process in the Kompot-KompotSpec pipeline might have led to inaccurate effective transit heights for this simulation. Nonetheless, KompotSpec manages to predict the major absorbers of Earth's atmosphere and the source of the diverging transit depths remains open for further study.

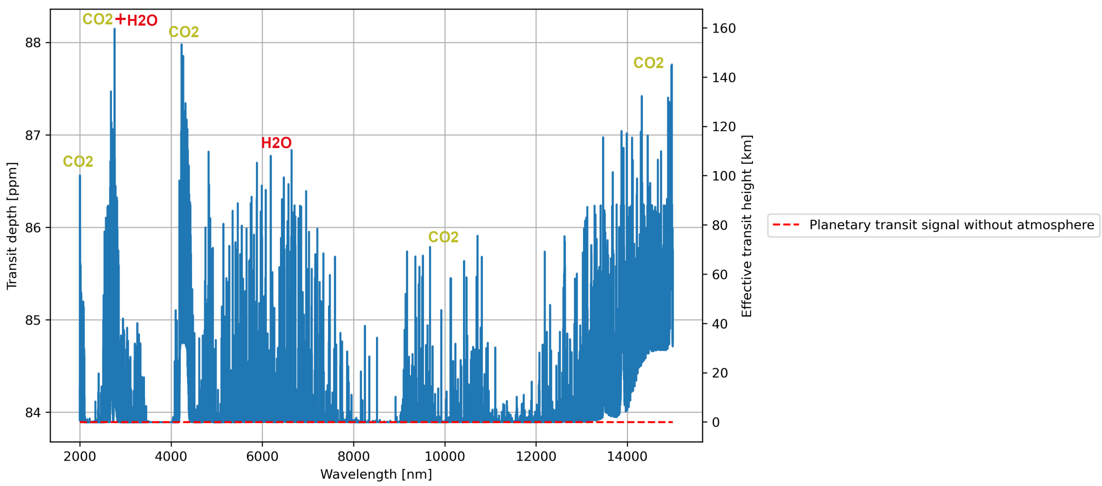

Figure 5.1.: Total transit spectra of Earth (No rebinning)

5.2. KompotSpec Titan simulation

Figure 5.2 combines the individual absorber transit spectra into one spectrum, making the KompotSpec effective transit heights comparable to Figure 4.5. The CH_4 features are listed in Table 5.1. While comparable for the feature at 3.3 μm, the features towards smaller wavelengths diverge farther from comparison data, probably at least in part to the effect of hazes not being replicated in KompotSpec's simulation. Still, all of the major CH_4 features can be reproduced by KompotSpec, with comparable transit depths for the biggest ones.

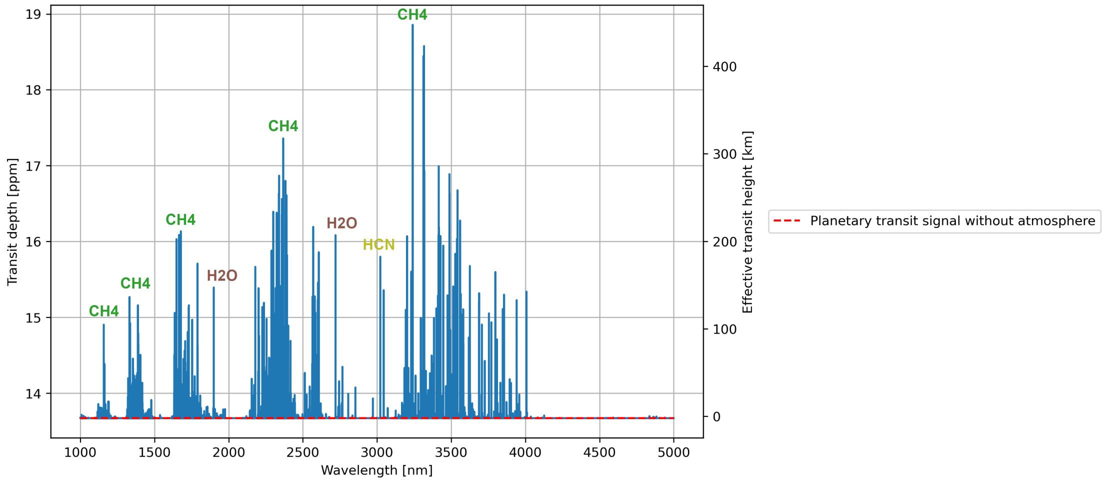

Figure 5.2.: Total transit spectra of Titan (No rebinning)

CH_4 Feature Wavelength [μm]	Effective transit height KompotSpec [km]	Effective transit height Robinson et al. (2014) [km]
1.2	100	295
1.4	135	285
1.7	200	275
2.3	300	300
3.3	420	360

Table 5.1.: Wavelengths and effective transit height of CH_4 features from KompotSpec and comparison data (Robinson et al., 2014)

5.3. Future prospects

While pressure broadening coefficients are included within the ExoMolOP data, they are not calculated anywhere in the current iteration of KompotSpec. This leads to very sharp absorption features, unlike those seen in, for example, JWST observations. Rebinning of these sharp absorption features from native spectral resolution to the spectral resolution of JWST's instruments therefore produces implausible results. Implementing this could make KompotSpec's results much more comparable to JWST's results. Implementing pressure broadening and sourcing coefficients for the Kompot/XUV mode can also be studied.

At the moment emission in the atmosphere is also not modeled in KompotSpec. However, the atmosphere itself also acts as a black-body which re-emits its own radiation in various wavelength regimes. This is especially important in the IR spectrum, since XUV radiation can heat up the atmosphere by adding energy to it. The release of this energy often occurs in the infrared. Modeling emission would open up Kompot and KompotSpec to investigate not only transit spectroscopy, but also emission spectroscopy. Implementation of scattering would also add another degree of realism and complexity to the simulated atmospheres and can be considered for further iterations of KompotSpec. While Mie scattering, which is a big factor for clouds and hazes (Pinhas and Madhusudhan, 2017), is common, Kompot acts above the cloud layer, meaning Rayleigh scattering should probably be prioritized.

The simulated light rays are as of now spread linearly between the lower to the upper KompotSpec simulation boundary. Due to Kompot's cell scaling the upper cells/layers are orders of magnitude larger than the lower ones. That results in even the lowest linearly spaced rays not probing the lowest atmospheric layers. This can be either solved by significantly increasing the number of simulated rays (which is computationally expensive). Alternatively the spacing could be changed to a non-linear spacing with greater light ray density at the bottom of the atmosphere leading to a more accurate simulation of the lower layers. Finally, As the focus of this work was to establish a radiative transfer extension to the Kompot code, scaleability and performance of the code were not the first priority. This should however be prioritized next, as many operations do not make use of optimized Python libraries such as *numpy*, which in the background run C code, which is much faster than pure Python, potentially reducing simulation times drastically.

5.4. Conclusion

This thesis has outlined contemporary knowledge of exoplanets and their atmospheres and how atmospheric models can be leveraged to interpret observational data. The Kompot model, used for studying the influence of XUV radiation on atmospheres and their evolutions has been summarized, with its limitations. KompotSpec, the main product of this thesis was developed to alleviate these limitations. By including the generation of synthetic transit spectra from Kompot data, and with the additional IR coverage enabled by the crosssections from the ExoMolOP project this thesis paves the way for Kompot models to be compared with observational data from contemporary instruments.

KompotSpec simulations have been compared against both Earth and Titan transit spectra in the previous sections. Especially the results for Titan were quite encouraging, given that this work did not consider the high altitude hazes likely to be encountered (Robinson et al., 2014). For Earth the results were somewhat different, not considering any prominent clouds or hazes, but instead more differences in the absorption of the cross-referenced features when compared to Lustig-Yaeger et al. (2023). This might be due to the much more complex P-T grid in the Earth simulation: While the Titan simulation uses just 2 different crosssections (each for a different P-T combination), the Earth simulation uses 208 different crosssections for the same reasons. The used P-T grid in combination with the associated crosssections might also just be too coarse, as currently each Kompot layer is assigned the unaltered ExoMolOP crosssection at the nearest P-T bin. Future work could look into interpolation of these crosssections or other methods to provide more continuous P-T dependent crosssection data for KompotSpec simulations.

The KompotSpec transit spectra also differ from the comparison transit spectra, since pressure broadening was not incorporated into KompotSpec. This leads to KompotSpec's transit spectrum having very sharp absorption features, that are not very broad. Which is unlike the real-world scenarios of both Earth and Titan where significant pressure leads to the broadening of the absorption features into absorption windows, which are easily visible in the transit spectra from the comparison data. This is also the reason no rebinned transit spectra were shown in this work, however exactly this would be needed to compare KompotSpec's transit spectra with spectra observed by JWST. Especially since the ExoMolOP crosssections KompotSpec uses have a spectral resolution R of 15000. The highest spectral resolution of JWST's NIRSpec is around 2700, and for most instruments much lower. Incorporating pressure broadening of the absorption lines, the pressure broadening coefficients already being available in the crosssection files, should be the highest priority in any future efforts to improve this work.

KompotSpec therefore signifies a much needed addition to the Kompot code, with a lot of future potential. By iterating both KompotSpec itself, as well as the Kompot simulations it builds upon, this work has made progress in enabling modeling of exoplanetary atmospheres in the age of JWST and infrared exoplanetary atmosphere studies.

Bibliography

Ahrer, E.-M., Alderson, L., Batalha, N. M., Batalha, N. E., Bean, J. L., Beatty, T. G., Bell, T. J., Benneke, B., Berta-Thompson, Z. K., Carter, A. L., Crossfield, I. J. M., Espinoza, N., Feinstein, A. D., Fortney, J. J., Gibson, N. P., Goyal, J. M., Kempton, E. M.-R., Kirk, J., Kreidberg, L., López-Morales, M., Line, M. R., Lothringer, J. D., Moran, S. E., Mukherjee, S., Ohno, K., Parmentier, V., Piaulet, C., Rustamkulov, Z., Schlawin, E., Sing, D. K., Stevenson, K. B., Wakeford, H. R., Allen, N. H., Birkmann, S. M., Brande, J., Crouzet, N., Cubillos, P. E., Damiano, M., Désert, J.-M., Gao, P., Harrington, J., Hu, R., Kendrew, S., Knutson, H. A., Lagage, P.-O., Leconte, J., Lendl, M., MacDonald, R. J., May, E. M., Miguel, Y., Molaverdikhani, K., Moses, J. I., Murray, C. A., Nehring, M., Nikolov, N. K., Petit dit de la Roche, D. J. M., Radica, M., Roy, P.-A., Stassun, K. G., Taylor, J., Waalkes, W. C., Wachiraphan, P., Welbanks, L., Wheatley, P. J., Aggarwal, K., Alam, M. K., Banerjee, A., Barstow, J. K., Blecic, J., Casewell, S. L., Changeat, Q., Chubb, K. L., Colón, K. D., Coulombe, L.-P., Daylan, T., de Val-Borro, M., Decin, L., Dos Santos, L. A., Flagg, L., France, K., Fu, G., García Muñoz, A., Gizis, J. E., Glidden, A., Grant, D., Heng, K., Henning, T., Hong, Y.-C., Inglis, J., Iro, N., Kataria, T., Komacek, T. D., Krick, J. E., Lee, E. K. H., Lewis, N. K., Lillo-Box, J., Lustig-Yaeger, J., Mancini, L., Mandell, A. M., Mansfield, M., Marley, M. S., Mikal-Evans, T., Morello, G., Nixon, M. C., Ortiz Ceballos, K., Piette, A. A. A., Powell, D., Rackham, B. V., Ramos-Rosado, L., Rauscher, E., Redfield, S., Rogers, L. K., Roman, M. T., Roudier, G. M., Scarsdale, N., Shkolnik, E. L., Southworth, J., Spake, J. J., Steinrueck, M. E., Tan, X., Teske, J. K., Tremblin, P., Tsai, S.-M., Tucker, G. S., Turner, J. D., Valenti, J. A., Venot, O., Waldmann, I. P., Wallack, N. L., Zhang, X., and Zieba, S. (2022). Identification of carbon dioxide in an exoplanet atmosphere. *Nature*, 614(7949):649–652.

Al-Refaie, A. F., Changeat, Q., Waldmann, I. P., and Tinetti, G. (2021). Taurex 3: A fast, dynamic, and extendable framework for retrievals. *The Astrophysical Journal*, 917(1):37.

Al-Refaie, A. F., Venot, O., Changeat, Q., and Edwards, B. (2024). Freckll: Full and reduced exoplanet chemical kinetics distilled.

Amerstorfer, U. V., Gröller, H., Lichtenegger, H., Lammer, H., Tian, F., Noack, L., Scherf, M., Johnstone, C., Tu, L., and Güdel, M. (2019). Escape and evolution of mars' co2 atmosphere: Influence of suprathermal atoms.

Bean, J. L., Kempton, E. M.-R., and Homeier, D. (2010). A ground-based transmission spectrum of the super-earth exoplanet gj 1214b. *Nature*, 468(7324):669–672.

Bellucci, A., Sicardy, B., Drossart, P., Rannou, P., Nicholson, P. D., Hedman, M., Baines, K. H., and Burrati, B. (2009). Titan solar occultation observed by Cassini/VIMS: Gas absorption and constraints on aerosol composition. *Icarus*, 201(1):198–216.

Bernath, P., Mcelroy, C., Abrams, M., Boone, C., Butler, M., Camy-Peyret, C., Carleer, M., Clerbaux, C., Coheur, P.-F., Colin, R., DeCola, P., Demazière, M., Drummond, J., Dufour, D., Evans, W., Fast, H., Fussen, D., Gilbert, K., Jennings, D., and Zou, J. (2005). Atmospheric chemistry experiment (ace): Mission overview. *Geophys. Res. Lett*, 32:15–1.

Blain, D., Charnay, B., and Bézard, B. (2021). 1d atmospheric study of the temperate sub-neptune k2-18b. *Astronomy & Astrophysics*, 646:A15.

Boone, C. D. and Bernath, P. F. (2019). The instrumental line shape of the atmospheric chemistry experiment Fourier transform spectrometer (ACE-FTS). *Journal of Quantitiative Spectroscopy and Radiative Trasfer*, 230:1–12.

Boro Saikia, S. (in prep.).

Catling, D. and Zahnle, K. (2009). The planetary air leak. *Scientific American*, 300:36–43.

Charbonneau, D., Brown, T. M., Latham, D. W., and Mayor, M. (2000). Detection of Planetary Transits Across a Sun-like Star. *Astrophysical Journal, Letters*, 529(1):L45–L48.

Charbonneau, D., Brown, T. M., Noyes, R. W., and Gilliland, R. L. (2002). Detection of an extrasolar planet atmosphere. *The Astrophysical Journal*, 568(1):377–384.

Chubb, K. L., Rocchetto, M., Yurchenko, S. N., Min, M., Waldmann, I., Barstow, J. K., Mollière, P., Al-Refaie, A. F., Phillips, M. W., and Tennyson, J. (2021). The exomolop database: Cross sections andk-tables for molecules of interest in high-temperature exoplanet atmospheres. *Astronomy & Astrophysics*, 646:A21.

Cloutier, R. (2024). Exoplanet demographics: Physical and orbital properties.

Cooper, C. S. and Showman, A. P. (2005). Dynamic meteorology at the photosphere of hd 209458b. *The Astrophysical Journal*, 629(1):L45–L48.

Del Genio, A. D., Kiang, N. Y., Way, M. J., Amundsen, D. S., Sohl, L. E., Fujii, Y., Chandler, M., Aleinov, I., Colose, C. M., Guzewich, S. D., and Kelley, M. (2019). Albedos, equilibrium temperatures, and surface temperatures of habitable planets. *The Astrophysical Journal*, 884(1):75.

Diamond-Lowe, H., Charbonneau, D., Malik, M., Kempton, E. M.-R., and Beletsky, Y. (2020). Optical transmission spectroscopy of the terrestrial exoplanet lhs 3844b from 13 ground-based transit observations. *The Astronomical Journal*, 160(4):188.

Doyon, R., Willott, C. J., Hutchings, J. B., Sivaramakrishnan, A., Albert, L., Lafreniere, D., Rowlands, N., Vila, M. B., Martel, A. R., LaMassa, S., Aldridge, D., Artigau, E., Cameron, P., Chayer, P., Cook, N. J., Cooper, R. A., Darveau-Bernier, A., Dupuis, J., Earnshaw, C., Espinoza, N., Filippazzo, J. C., Fullerton, A. W., Gaudreau, D., Gawlik, R., Goudfrooij, P., Haley, C., Kammerer, J., Kendall, D., Lambros, S. D., Ignat, L. I., Maszkiewicz, M., McColgan, A., Morishita, T., Ouellette, N. N. Q., Pacifici, C., Philippi, N., Radica, M., Ravindranath, S., Rowe, J., Roy, A., Saad, K., Sohn, S. T., Talens, G. J., Thatte, D., Taylor, J. M., Vandal, T., Volk, K., Wander, M., Warner, G., Zheng, S.-H., Zhou, J., Abraham, R., Beaulieu, M., Benneke, B., Ferrarese, L., Johnstone, D., Kaltenegger, L., Meyer, M. R., Pipher, J. L., Rameau, J., Rieke, M., Salhi, S., and Sawicki, M. (2023). The near infrared imager and slitless spectrograph for the james webb space telescope – i. instrument overview and in-flight performance.

Fraine, J., Deming, D., Benneke, B., Knutson, H., Jordán, A., Espinoza, N., Madhusudhan, N., Wilkins, A., and Todorov, K. (2014). Water vapour absorption in the clear atmosphere of a neptune-sized exoplanet. *Nature*, 513(7519):526–529.

Fritzewski, D. J., Barnes, S. A., James, D. J., Järvinen, S. P., and Strassmeier, K. G. (2021). A detailed understanding of the rotation-activity relationship using the 300 Myr old open cluster NGC 3532. *Astronomy and Astrophysics*, 656:A103.

Fulton, B. J., Petigura, E. A., Howard, A. W., Isaacson, H., Marcy, G. W., Cargile, P. A., Hebb, L., Weiss, L. M., Johnson, J. A., Morton, T. D., Sinukoff, E., Crossfield, I. J. M., and Hirsch, L. A. (2017). The california-kepler survey. iii. a gap in the radius distribution of small planets*. *The Astronomical Journal*, 154(3):109.

Gupta, A. and Schlichting, H. E. (2019). Sculpting the valley in the radius distribution of small exoplanets as a by-product of planet formation: the core-powered mass-loss mechanism. *Monthly Notices of the Royal Astronomical Society*, 487(1):24–33.

Helling, C., Ackerman, A., Allard, F., Dehn, M., Hauschildt, P., Homeier, D., Lodders, K., Marley, M., Rietmeijer, F., Tsuji, T., and Woitke, P. (2008a). A comparison of chemistry and dust cloud formation in ultracool dwarf model atmospheres. *Monthly Notices of the Royal Astronomical Society*, 391(4):1854–1873.

Helling, C., Dehn, M., Woitke, P., and Hauschildt, P. (2008b). Consistent simulations of substellar atmospheres and nonequilibrium dust cloud formation. *Astrophysical Journal Letters*, 675(2):L105–L108. Note related output below contains correction of this paper.

Henry, G. W., Marcy, G. W., Butler, R. P., and Vogt, S. S. (2000). A Transiting "51 Peg-like" Planet. *Astrophysical Journal, Letters*, 529(1):L41–L44.

Holmberg, Måns and Madhusudhan, Nikku (2024). Possible hycean conditions in the sub-neptune toi-270 d. *A&A*, 683:L2.

Hu, R., Bello-Arufe, A., Zhang, M., Paragas, K., Zilinskas, M., van Buchem, C., Bess, M., Patel, J., Ito, Y., Damiano, M., Scheucher, M., Oza, A. V., Knutson, H. A., Miguel, Y., Dragomir, D., Brandeker, A., and Demory, B.-O. (2024). A secondary atmosphere on the rocky exoplanet 55 cancri e. *Nature*, 630(8017):609–612.

Hughes, R., Bernath, P. F., and Boone, C. D. (2014). Ace infrared spectral atlases of the earth's atmosphere. *Journal of Quantitative Spectroscopy & Radiative Transfer*, 148:18–21.

Ih, J., Kempton, E. M.-R., Whittaker, E. A., and Lessard, M. (2023). Constraining the thickness of trappist-1 b's atmosphere from its jwst secondary eclipse observation at 15 micrometer. *The Astrophysical Journal Letters*, 952(1):L4.

Ionov, D. E. and Shematovich, V. I. (2015). Hydrogen-dominated upper atmosphere of an exoplanet: Heating by stellar radiation from soft X-rays to extreme ultraviolet. *Solar System Research*, 49(5):339–345.

Jackson, B., Barnes, R., and Greenberg, R. (2008). Tidal heating of terrestrial extra-solar planets and implications for their habitability. *Monthly Notices of the Royal Astronomical Society*, 391(1):237–245.

Jakobsen, P., Ferruit, P., Alves de Oliveira, C., Arribas, S., Bagnasco, G., Barho, R., Beck, T. L., Birkmann, S., Böker, T., Bunker, A. J., Charlot, S., de Jong, P., de Marchi, G., Ehrenwinkler, R., Falcolini, M., Fels, R., Franx, M., Franz, D., Funke, M., Giardino, G., Gnata, X., Holota, W., Honnen, K., Jensen, P. L., Jentsch, M., Johnson, T., Jollet, D., Karl, H., Kling, G., Köhler, J., Kolm, M.-G., Kumari, N., Lander, M. E., Lemke, R., López-Caniego, M., Lützgendorf, N., Maiolino, R., Manjavacas, E., Marston, A., Maschmann, M., Maurer, R., Messerschmidt, B., Moseley, S. H., Mosner, P., Mott, D. B., Muzerolle, J., Pirzkal, N., Pittet, J.-F., Plitzke, A., Posselt, W., Rapp, B., Rauscher, B. J., Rawle, T., Rix, H.-W., Rödel, A., Rumler, P., Sabbi, E., Salvignol, J.-C., Schmid, T., Sirianni, M., Smith, C., Strada, P., te Plate, M., Valenti, J., Wettemann, T., Wiehe, T., Wiesmayer, M., Willott, C. J., Wright, R., Zeidler, P., and Zincke, C. (2022). The near-infrared spectrograph (nirspec) on thejames webbspace telescope: I. overview of the instrument and its capabilities. *Astronomy & Astrophysics*, 661:A80.

Johnstone, C. (2018). The Kompot Code: first-principles upper atmosphere modelling and the evolution of planetary atmospheres. In *European Planetary Science Congress*, pages EPSC2018–1054.

Johnstone, C., Güdel, M., Lammer, H., and Kislyakova, K. (2018). Upper atmospheres of terrestrial planets: Carbon dioxide cooling and the earth's thermospheric evolution. *Astronomy & Astrophysics*, 617. Publisher Copyright: © 2018 ESO.

Johnstone, C. P. (2021). Stellar winds and planetary atmospheres.

Johnstone, C. P., Bartel, M., and Güdel, M. (2021a). The active lives of stars: A complete description of the rotation and xuv evolution of f, g, k, and m dwarfs. *Astronomy & Astrophysics*, 649:A96.

Johnstone, C. P., Khodachenko, M. L., Lüftinger, T., Kislyakova, K. G., Lammer, H., and Güdel, M. (2019). Extreme hydrodynamic losses of earth-like atmospheres in the habitable zones of very active stars. *Astronomy & Astrophysics*, 624:L10.

Johnstone, C. P., Lammer, H., Kislyakova, K. G., Scherf, M., and Güdel, M. (2021b). The young sun's xuv-activity as a constraint for lower co2-limits in the earth's archean atmosphere. *Earth and Planetary Science Letters*, 576:117197.

Jordán, A., Espinoza, N., Rabus, M., Eyheramendy, S., Sing, D., Désert, J., Bakos, G., Fortney, J., López-Morales, M., Maxted, P., Triaud, A., and Szentgyorgyi, A. (2013). A ground-based optical transmission spectrum of wasp-6b. *Astrophysical Journal*, 778(2).

Kataria, T., Showman, A. P., Fortney, J. J., Marley, M. S., and Freedman, R. S. (2014). The Atmospheric Circulation of the Super Earth GJ 1214b: Dependence on Composition and Metallicity. *Astrophysical Journal*, 785(2):92.

Kite, E. S., Fegley Jr., B., Schaefer, L., and Ford, E. B. (2020). Atmosphere origins for exoplanet sub-neptunes. *The Astrophysical Journal*, 891(2):111.

Knutson, H. A., Benneke, B., Deming, D., and Homeier, D. (2014). A featureless transmission spectrum for the neptune-mass exoplanet gj 436b. *Nature*, 505(7481):66–68.

Lecavelier des Etangs, A., Pont, F., Vidal-Madjar, A., and Sing, D. (2008). Rayleigh scattering in the transit spectrum of hd 189733b. *Astronomy & Astrophysics*, 481(2):L83–L86.

Li, M. and Xiao, L. (2016). Lifetimes and Accretion Rates of Protoplanetary Disks. *Astrophysical Journal*, 820(1):36.

Lim, O., Benneke, B., Doyon, R., MacDonald, R. J., Piaulet, C., Artigau, E., Coulombe, L.-P., Radica, M., L'Heureux, A., Albert, L., Rackham, B. V., de Wit, J., Salhi, S., Roy, P.-A., Flagg, L., Fournier-Tondreau, M., Taylor, J., Cook, N. J., Lafrenière, D., Cowan, N. B., Kaltenegger, L., Rowe, J. F., Espinoza, N., Dang, L., and Darveau-Bernier, A. (2023). Atmospheric reconnaissance of trappist-1 b with jwst/niriss: Evidence for strong stellar contamination in the transmission spectra. *The Astrophysical Journal Letters*, 955(1):L22.

Lopez, E. D. and Fortney, J. J. (2014). Understanding the mass-radius relation for sub-neptunes: Radius as a proxy for composition. *The Astrophysical Journal*, 792(1):1.

Lundin, R., Lammer, H., and Ribas, I. (2007). Planetary Magnetic Fields and Solar Forcing: Implications for Atmospheric Evolution. *Space Science Reviews*, 129(1-3):245–278.

Lustig-Yaeger, J., Meadows, V. S., Crisp, D., Line, M. R., and Robinson, T. D. (2023). Earth as a transiting exoplanet: A validation of transmission spectroscopy and atmospheric retrieval methodologies for terrestrial exoplanets.

Macdonald, E. J. R. and Cowan, N. B. (2019). An empirical infrared transit spectrum of earth: opacity windows and biosignatures. *Monthly Notices of the Royal Astronomical Society*, 489(1):196–204.

MacDonald, R. J. and Batalha, N. E. (2023). A catalog of exoplanet atmospheric retrieval codes. *Research Notes of the AAS*, 7(3):54.

Madhusudhan, N., Sarkar, S., Constantinou, S., Holmberg, M., Piette, A. A. A., and Moses, J. I. (2023). Carbon-bearing molecules in a possible hycean atmosphere.

Maggio, A., Pillitteri, I., Argiroffi, C., Locci, D., Benatti, S., and Micela, G. (2024). Xuv irradiation of young planetary atmospheres. results from a joint xmm-newton and hst observation of hip67522. *Astronomy & Astrophysics*, 690:A383.

Maltagliati, L., Bézard, B., Vinatier, S., Hedman, M. M., Lellouch, E., Nicholson, P. D., Sotin, C., de Kok, R. J., and Sicardy, B. (2015). Titan's atmosphere as observed by cassini/vims solar occultations: Ch4, co and evidence for c2h6 absorption. *Icarus*, 248:1–24.

Mayor, M. and Queloz, D. (1995). A Jupiter-mass companion to a solar-type star. *Nature*, 378(6555):355–359.

Mendonça, J. M. (2019). Angular momentum and heat transport on tidally locked hot jupiter planets. *Monthly Notices of the Royal Astronomical Society*, 491(1):1456–1470.

Misener, W., Schlichting, H. E., and Young, E. D. (2023). Atmospheres as windows into sub-neptune interiors: coupled chemistry and structure of hydrogen–silane–water envelopes. *Monthly Notices of the Royal Astronomical Society*, 524(1):981–992.

Mollière, P., Wardenier, J. P., van Boekel, R., Henning, T., Molaverdikhani, K., and Snellen, I. A. G. (2019). petitradtrans: A python radiative transfer package for exoplanet characterization and retrieval. *Astronomy & Astrophysics*, 627:A67.

Morley, C. V., Fortney, J. J., Marley, M. S., Zahnle, K. J., Line, M. R., Kempton, E. M.-R., Lewis, N. K., and Cahoy, K. L. (2015). Seeing through the clouds: Thermal emission and reflected light spectra of super-earths with flat transmission spectra.

Morley, C. V., Knutson, H., Line, M., Fortney, J. J., Thorngren, D., Marley, M. S., Teal, D., and Lupu, R. (2017). Forward and inverse modeling of the emission and transmission spectrum of gj 436b: Investigating metal enrichment, tidal heating, and clouds. *The Astronomical Journal*, 153(2):86.

Mousis, O., Deleuil, M., Aguichine, A., Marcq, E., Naar, J., Aguirre, L. A., Brugger, B., and Gonçalves, T. (2020). Irradiated ocean planets bridge super-earth and sub-neptune populations. *The Astrophysical Journal Letters*, 896(2):L22.

O'Neill, C., O'Neill, H. S. C., and Jellinek, A. M. (2020). On the Distribution and Variation of Radioactive Heat Producing Elements Within Meteorites, the Earth, and Planets. *Space Science Reviews*, 216(3):37.

Owen, J. E. and Wu, Y. (2013). Keplerplanets: A tale of evaporation. *The Astrophysical Journal*, 775(2):105.

Owen, J. E. and Wu, Y. (2017). The evaporation valley in the kepler planets. *The Astrophysical Journal*, 847(1):29.

Pinhas, A. and Madhusudhan, N. (2017). On signatures of clouds in exoplanetary transit spectra. *Monthly Notices of the RAS*, 471(4):4355–4373.

Rannou, P., Montmessin, F., Hourdin, F., and Lebonnois, S. (2006). The Latitudinal Distribution of Clouds on Titan. *Science*, 311(5758):201–205.

Ransford, G. (1982). The accretional heating of the terrestrial planets: a review. *Physics of the Earth and Planetary Interiors*, 29(3):209–217.

Robinson, T. D., Maltagliati, L., Marley, M. S., and Fortney, J. J. (2014). Titan solar occultation observations reveal transit spectra of a hazy world. *Proceedings of the National Academy of Sciences*, 111(25):9042–9047.

Sanz-Forcada, J., Micela, G., Ribas, I., Pollock, A. M. T., Eiroa, C., Velasco, A., Solano, E., and García-Álvarez, D. (2011). Estimation of the XUV radiation onto close planets and their evaporation. *Astronomy and Astrophysics*, 532:A6.

Sanz-Forcada, J., Micela, G., Ribas, I., Pollock, A. M. T., Eiroa, C., Velasco, A., Solano, E., and García-Álvarez, D. (2011). Estimation of the xuv radiation onto close planets and their evaporation. *A&A*, 532:A6.

Sarkar, S., Madhusudhan, N., Constantinou, S., and Holmberg, M. (2024). Exoplanet transit spectroscopy with jwst nirspec: Diagnostics and homogeneous case study of wasp-39 b.

Schlichting, H. and Mukhopadhyay, S. (2018). Atmosphere impact losses. *Space Science Reviews*, 214.

Shematovich, V. I. and Marov, M. Y. (2018). Escape of planetary atmospheres: physical processes and numerical models. *Physics Uspekhi*, 61(3):217.

Shorttle, O., Jordan, S., Nicholls, H., Lichtenberg, T., and Bower, D. J. (2024). Distinguishing oceans of water from magma on mini-neptune k2-18b. *The Astrophysical Journal Letters*, 962(1):L8.

Sing, D. K., Fortney, J. J., Nikolov, N., Wakeford, H. R., Kataria, T., Evans, T. M., Aigrain, S., Ballester, G. E., Burrows, A. S., Deming, D., Désert, J.-M., Gibson, N. P., Henry, G. W., Huitson, C. M., Knutson, H. A., Etangs, A. L. d., Pont, F., Showman, A. P., Vidal-Madjar, A., Williamson, M. H., and Wilson, P. A. (2015). A continuum from clear to cloudy hot-jupiter exoplanets without primordial water depletion. *Nature*, 529(7584):59–62.

Stock, J. W., Kitzmann, D., Patzer, A. B. C., and Sedlmayr, E. (2018). Fastchem: A computer program for efficient complex chemical equilibrium calculations in the neutral/ionized gas phase with applications to stellar and planetary atmospheres. *Monthly Notices of the Royal Astronomical Society.*

Swain, M. R., Vasisht, G., Tinetti, G., Bouwman, J., Chen, P., Yung, Y., Deming, D., and Deroo, P. (2008). Molecular signatures in the near infrared dayside spectrum of hd 189733b.

Taylor, J., Radica, M., Welbanks, L., MacDonald, R. J., Blecic, J., Zamyatina, M., Roth, A., Bean, J. L., Parmentier, V., Coulombe, L.-P., Feinstein, A. D., Espinoza, N., Benneke, B., Lafrenière, D., Doyon, R., and Ahrer, E.-M. (2023). Awesome soss: atmospheric characterization of wasp-96b using the jwst early release observations. *Monthly Notices of the Royal Astronomical Society*, 524(1):817–834.

Tsai, S.-M., Lee, E. K. H., Powell, D., Gao, P., Zhang, X., Moses, J., Hébrard, E., Venot, O., Parmentier, V., Jordan, S., Hu, R., Alam, M. K., Alderson, L., Batalha, N. M., Bean, J. L., Benneke, B., Bierson, C. J., Brady, R. P., Carone, L., Carter, A. L., Chubb, K. L., Inglis, J., Leconte, J., Line, M., López-Morales, M., Miguel, Y., Molaverdikhani, K., Rustamkulov, Z., Sing, D. K., Stevenson, K. B., Wakeford, H. R., Yang, J., Aggarwal, K., Baeyens, R., Barat, S., de Val-Borro, M., Daylan, T., Fortney, J. J., France, K., Goyal, J. M., Grant, D., Kirk, J., Kreidberg, L., Louca, A., Moran, S. E., Mukherjee, S., Nasedkin, E., Ohno, K., Rackham, B. V., Redfield, S., Taylor, J., Tremblin, P., Visscher, C., Wallack, N. L., Welbanks, L., Youngblood, A., Ahrer, E.-M., Batalha, N. E., Behr, P., Berta-Thompson, Z. K., Blecic, J., Casewell, S. L., Crossfield, I. J. M., Crouzet, N., Cubillos, P. E., Decin, L., Désert, J.-M., Feinstein, A. D., Gibson, N. P., Harrington, J., Heng, K., Henning, T., Kempton, E. M.-R., Krick, J., Lagage, P.-O., Lendl, M., Lothringer, J. D., Mansfield, M., Mayne, N. J., Mikal-Evans, T., Palle, E., Schlawin, E., Shorttle, O., Wheatley, P. J., and Yurchenko, S. N. (2023). Photochemically produced so2 in the atmosphere of wasp-39b. *Nature*, 617(7961):483–487.

Tsai, S.-M., Malik, M., Kitzmann, D., Lyons, J. R., Fateev, A., Lee, E., and Heng, K. (2021). A comparative study of atmospheric chemistry with vulcan. *The Astrophysical Journal*, 923(2):264.

Tsiaras, A., Waldmann, I. P., Tinetti, G., Tennyson, J., and Yurchenko, S. N. (2019). Water vapour in the atmosphere of the habitable-zone eight-earth-mass planet k2-18 b. *Nature Astronomy*, 3(12):1086–1091.

Tsuji, T. (1973). Molecular abundances in stellar atmospheres. II. *Astronomy and Astrophysics*, 23:411.

Van Looveren, G., Güdel, M., Boro Saikia, S., and Kislyakova, K. (2024). Airy worlds or barren rocks? on the survivability of secondary atmospheres around the trappist-1 planets. *Astronomy & Astrophysics.*

Venturini, J. and Helled, R. (2017). The formation of mini-neptunes. *The Astrophysical Journal*, 848(2):95.

Waldmann, I. P., Tinetti, G., Rocchetto, M., Barton, E. J., Yurchenko, S. N., and Tennyson, J. (2015). Tau-rex i: A next generation retrieval code for exoplanetary atmospheres. *The Astrophysical Journal*, 802(2):107.

Way, M. J., Aleinov, I., Amundsen, D. S., Chandler, M. A., Clune, T. L., Genio, A. D. D., Fujii, Y., Kelley, M., Kiang, N. Y., Sohl, L., and Tsigaridis, K. (2017). Resolving orbital and climate keys of earth and extraterrestrial environments with dynamics (rocke-3d) 1.0: A general circulation model for simulating the climates of rocky planets. *The Astrophysical Journal Supplement Series*, 231(1):12.

Williams, J. P. and Cieza, L. A. (2011). Protoplanetary disks and their evolution. *Annual Review of Astronomy and Astrophysics*, 49(1):67–117.

Winn, J. N. (2014). Transits and occultations.

Woitke, P., Helling, C., Hunter, G. H., Millard, J. D., Turner, G. E., Worters, M., Blecic, J., and Stock, J. W. (2018). Equilibrium chemistry down to 100 k: Impact of silicates and phyllosilicates on the carbon to oxygen ratio. *Astronomy & Astrophysics*, 614:A1.

Wolf, E. T., Kopparapu, R., Airapetian, V., Fauchez, T., Guzewich, S. D., Kane, S. R., Pidhorodetska, D., Way, M. J., Abbot, D. S., Checlair, J. H., Davis, C. E., Genio, A. D., Dong, C., Eggl, S., Fleming, D. P., Fujii, Y., Haghighipour, N., Heavens, N., Henning, W. G., Kiang, N. Y., Lopez-Morales, M., Lustig-Yaeger, J., Meadows, V., Reinhard, C. T., Rugheimer, S., Schwieterman, E. W., Shields, A. L., Sohl, L., Turbet, M., and Wordsworth, R. D. (2019). The importance of 3d general circulation models for characterizing the climate and habitability of terrestrial extrasolar planets.

Wolszczan, A. and Frail, D. A. (1992). A planetary system around the millisecond pulsar PSR1257 + 12. *Nature*, 355(6356):145–147.

Wordsworth, R. and Kreidberg, L. (2022). Atmospheres of rocky exoplanets. *Annual Review of Astronomy and Astrophysics*, 60(1):159–201.

Xue, Q., Bean, J. L., Zhang, M., Mahajan, A., Ih, J., Eastman, J. D., Lunine, J., Mansfield, M. W., Coy, B. P., Kempton, E. M.-R., Koll, D., and Kite, E. (2024). Jwst thermal emission of the terrestrial exoplanet gj 1132b. *The Astrophysical Journal Letters*, 973(1):L8.

Zeng, L., Jacobsen, S. B., Sasselov, D. D., Petaev, M. I., Vanderburg, A., Lopez-Morales, M., Perez-Mercader, J., Mattsson, T. R., Li, G., Heising, M. Z., Bonomo, A. S., Damasso, M., Berger, T. A., Cao, H., Levi, A., and Wordsworth, R. D. (2019). Growth model interpretation of planet size distribution. *Proceedings of the National Academy of Sciences*, 116(20):9723–9728.

Zieba, S., Kreidberg, L., Ducrot, E., Gillon, M., Morley, C., Schaefer, L., Tamburo, P., Koll, D. D. B., Lyu, X., Acuña, L., Agol, E., Iyer, A. R., Hu, R., Lincowski, A. P., Meadows, V. S., Selsis, F., Bolmont, E., Mandell, A. M., and Suissa, G. (2023). No thick carbon dioxide atmosphere on the rocky exoplanet trappist-1 c. *Nature*, 620(7975):746–749.

Acronyms

ACE-FTS Atmospheric Chemistry Experiment Fourier Transform Spectrometer. 30

CE Chemical Equilibrium. 9, 10

GCM General Circulation Model. 10

HST Hubble Space Telescope. 4, 10

HZ Habitable Zone. xii, 53–56

I/O Input/Output. 61

IR Infrared. iii, v, 13, 22, 25, 29, 32, 37, 59

IRAC Infrared Array Camera. 4

JWST James Webb Space Telescope. 4, 5, 8–10, 19, 30, 36–38

MCMC Markov Chain Monte Carlo. 9

NICMOS Near Infrared Camera and Multi-Object Spectrometer. 4

NIRISS Near Infrared Imager and Slitless Spectrograph. 4

NIRSpec Near-Infrared Spectrograph. 4, 38

P-T Pressure-Temperature. xi, 20, 25, 27, 30, 31, 38, 59

RV Radial Velocity. 1

SCISAT Scientific Satellite. 30

UV Ultraviolet. iii, v, 7, 19, 22, 24, 25, 59

VIMS Visual and Infrared Mapping Spectrometer. 33

WFC3 Wide Field Camera 3. 4

XUV X-Ray and Ultraviolet. xii, 5, 7, 8, 13, 14, 19, 24, 37, 53–57

Glossary

Cassini Space probe observing Saturn and its moons from 2004 to 2017. xii, 33, 34

ExoMol Database of molecular line lists, used for spectra characterization of atmospheres. 9, 24, 29, 32, 51

ExoMolOP Database of opacities for molecules of astrophysical interest, based upon ExoMol, HITEMP and MoLLIST. iii, v, 19, 24, 25, 29, 36–38, 59, 61

HITEMP Spin-off of HITRAN for higher temperatures, used for atmospheric studies. 9, 24, 51

HITRAN Database of spectroscopic parameters of molecules, used for atmospheric studies. 9, 24, 51

Kompot Simulation code for planetary atmosphere evolution in the radiation environment of the host star. iii, v, xi, xii, 9–11, 13–16, 19, 20, 22, 24–26, 29, 32, 35, 37, 38, 51, 59, 61, 64–67, 70–73

KompotSpec Extension code to Kompot, adding radiative transfer to produce synthetic transit spectra. iii, v, vii, ix, xi, 9–11, 19, 20, 22, 24–26, 28–33, 35–38, 59, 61

MoLLIST Database of molecular line lists, intensities and spectra. 24, 51

NIST United States government agency, also provides spectroscopic data. 24

petitRADTRANS Code built for spectral characterization of exoplanet atmospheres. 9, 19

Spitzer Spitzer Space Telescope, observing in the infrared wavelengths from 2003 to 2020. 4, 10

TauREx Atmospheric retrieval framework utilizing radiative transfer. 9, 19, 25

A. Stellar evolution and influence on planetary atmospheres

The influence of the long-term evolution of the host star on its planet's atmosphere is not very self-explanatory but hugely important over the lifetime of the planetary system, which is why we want to examine this effect more closely. Before we do that however, lets examine where the most radiation is absorbed in a planet's atmosphere in Figure A.1 (this figure is a simulation based on a modern Earth/Sun system). As can be seen the range from 0 to 1000 Å is basically completely absorbed at heights of 110 km or above (red line in Figure A.1), therefore in the top of Earth's thermosphere and all of its exosphere. These atmospheric layers are mainly composed of hydrogen and helium, meaning they are the first to be stripped from the XUV irradiation of the star. In this modern, relatively low-XUV scenario Earth loses about three kilograms of atmospheric gas (mostly hydrogen, a little helium and trace elements) per second Catling and Zahnle (2009).

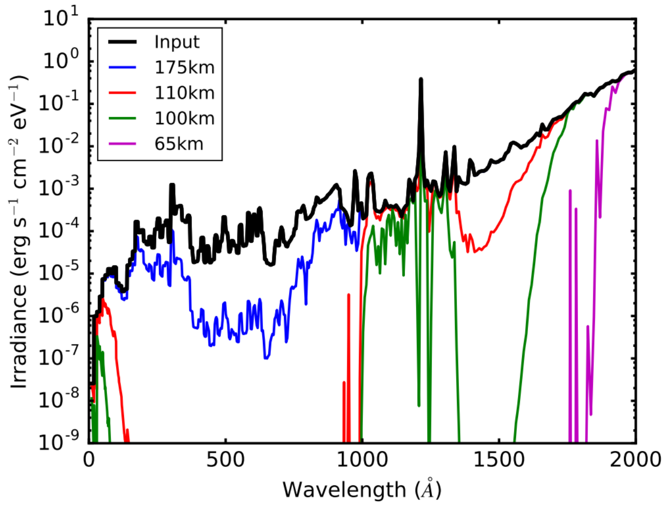

Figure A.1.: Simulated XUV throughput at different altitudes in a modern Earth/Sun system, Source: Johnstone et al. (2018)

However the low XUV losses are for our modern Sun. If we compare XUV flux density in the Habitable Zone (HZ) of a more active Sun (earlier in its evolution) or a typical M dwarf (the most numerous type of star in the galaxy) in Figure A.2 the picture changes. The figure shows that more active stages in the Sun's evolution have seen XUV flux densities on the order of two magnitudes higher than today's flux density. This results in significantly higher XUV absorption in the upper atmosphere and therefore increased atmospheric loss rates. The higher XUV irradiation also holds true for M dwarfs, the most numerous stars in the galaxy, and the easiest to detect a transiting exoplanet around.

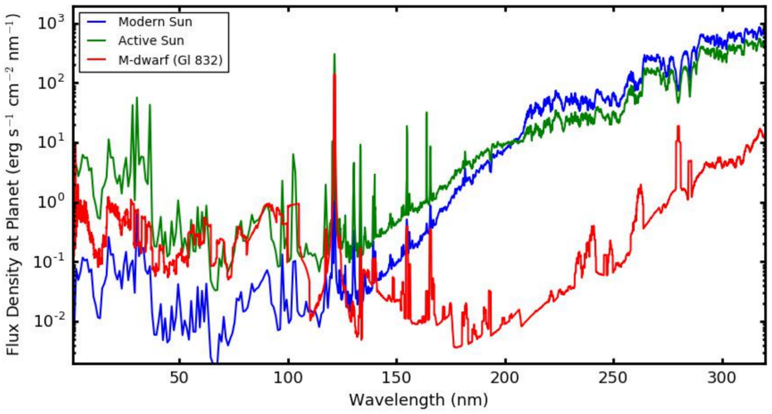

Figure A.2.: XUV flux density in HZ for a modern Sun, the Sun earlier during its more active phases and an M dwarf, Source: Johnstone (2021)

So far we have established the following:

- Stellar irradiation can erode/strip the atmosphere
- XUV radiation seems to be the easiest way to strip the upper layers of the atmosphere
    - Significant amounts of XUV are output by most stars (especially early in their evolution)
- XUV affects the upper layers of the atmosphere where light elements are easily removed

However the XUV irradiation is also significantly higher at the beginning of a star's life (as the high initial rotation rate leads to high activity) and only decreases over the star's lifetime. How fast/slow this process occurs, how high the expected XUV radiation levels are and what the underlying principles to this are, is outlined in the paragraphs below.

Stars are born with a wide range of rotational rates (see observations for different clusters of different ages in Figure A.3), however over time stars lower their rotation rate. Generally it is observed that when a star's rotation rate decreases (one cause of this being angular momentum losses to stellar winds), its stellar activity also decreases Fritzewski et al. (2021). This is thought to occur because of a process called the solar dynamo (the explanation of which is beyond the scope of this introduction). What is notable is that all stars of a fixed mass (independent of their initial rotation rate) seem to evolve towards a singe final rotation rate (as seen in the 2500 Myr panel of

Figure A.3), only dependent on their mass. Generally the rotation rates of more massive stars settle much quicker than those of less massive stars. This can be seen be seen in the panels for 650, 1000 and 2500 Myrs in Figure A.3 where the scatter for lower mass stars is much more pronounced than the scatter for stars of approximately lower mass.

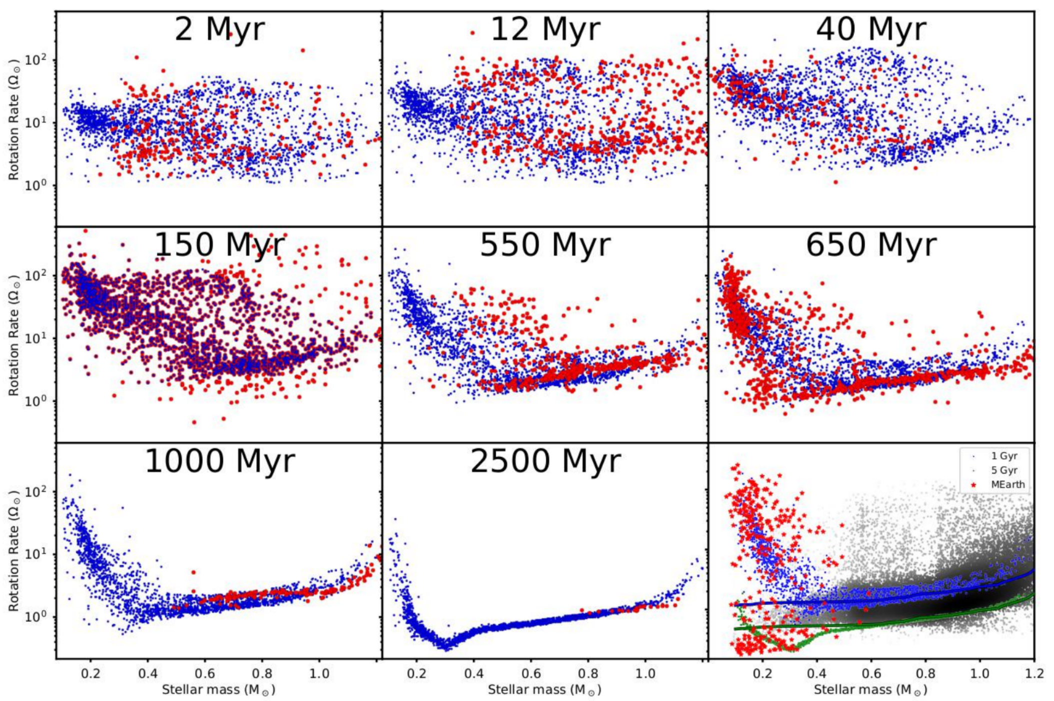

Figure A.3.: Observations of clusters of different ages (one panel = one cluster) and their stellar population's mass (x-Axis of each panel) and stellar rotation rate (y-Axis of each panel), Source: Johnstone et al. (2021a)

To reinforce this point let's consider Figure A.4. Here it can be seen that the evolutionary paths for fast, average and slow rotators have mostly converged for all but the lightest stars after approximately 2 Gyrs. Indeed the M-dwarfs have not had time to fully spin down even after billions of years. Figure A.4 also illustrates well that it is uncertain whether our own Sun was a fast, average or slow rotator (though it is suggested to have been a slow rotator with little activity in Johnstone et al. (2021b) using atmospheric simulations instead of relying on stellar rotation rates). Since it is much older than the time needed for the rotation rates to converge, today's solar rotation rate does not offer any hints as to how fast the Sun rotated / how active the Sun was early on.

If we recall that high rotation rate corresponds to higher stellar activity, we can therefore combine that high rotation rate corresponds to a higher XUV-radiation. And indeed when observing the XUV luminosity and XUV flux in the HZ for stars of dif-

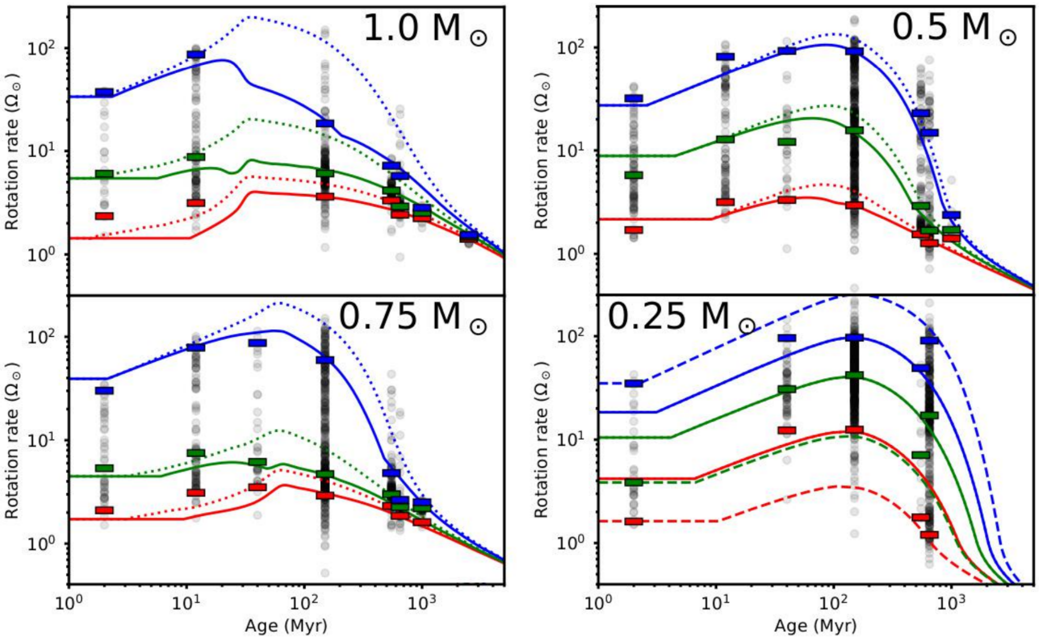

Figure A.4.: Rotation rate evolution paths for stars of different mass; Blue lines: 95th percentile of rotation rate ("Fast Rotators"); Red lines: median rotation rate; Green lines: 5th percentile of rotation rate ("Slow Rotators"), Source: Johnstone et al. (2021a)

ferent masses in Figure A.5 it can clearly be seen that fast rotators have higher levels of XUV output over longer timescales. What is possibly even more interesting is if the secondary y-Axis in Figure A.5 is considered: even though their XUV luminosities are smaller, the XUV flux in the HZ is considerably larger (by up to a magnitude) for the smaller M-dwarfs, with dramatic consequences for possible atmospheres or habitability.

In conclusion, when studying potential exoplanetary atmospheres, the host star is of the utmost importance. Size, mass, lifetime and spectral type maybe of great importance, but XUV activity over the stellar lifetime (and by proxy evolution of its rotation rate / stellar activity) also do need to be considered.

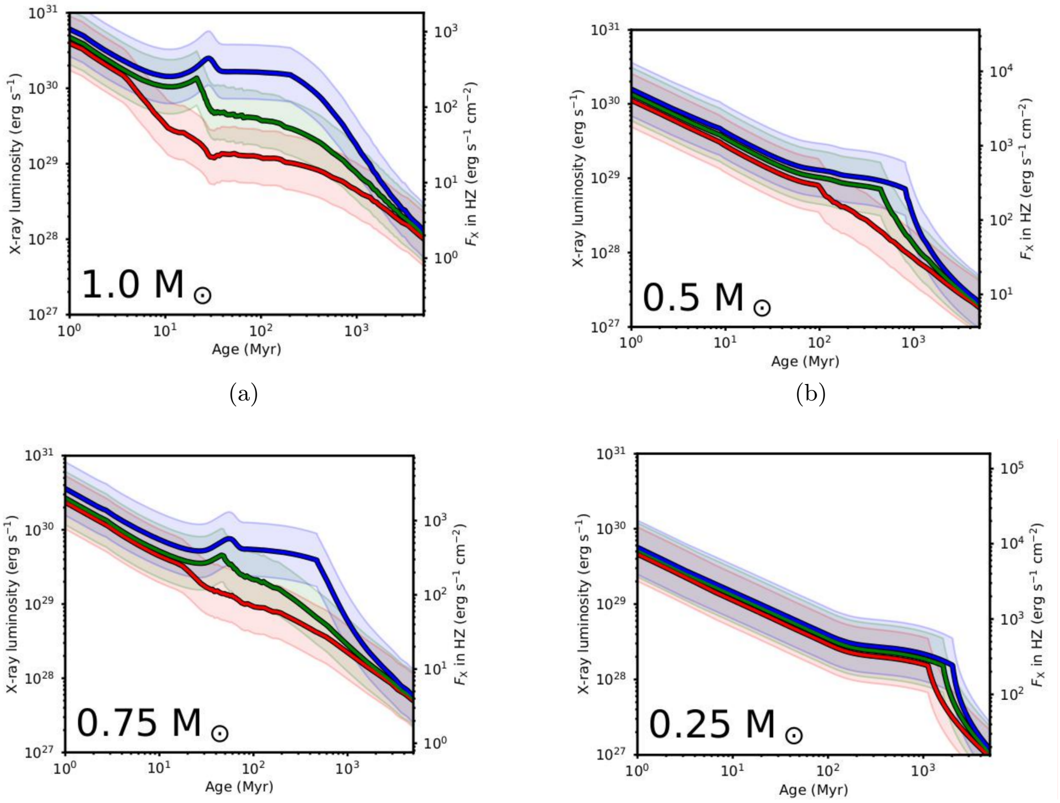

(a) (b) (c) (d)

Figure A.5.: XUV activity of stars of different maths and rotation rate evolutions; Blue lines: 95th percentile of rotation rate ("Fast Rotators"); Red lines: median rotation rate; Green lines: 5th percentile of rotation rate ("Slow Rotators"), Source: Johnstone et al. (2021a)

B. KompotSpec Configuration parameters

Variable Name	Parameter description
GRID_FILENAME	Relative path to Kompot file containing atmospheric cells and structure
SPECIES_FILENAME	Relative path to Kompot file with absorber densities
KOMPOT_CROSSSECTION_FILENAME	Relative path to Kompot file containing UV crosssections
THERMALPROPERTIES_FILENAME	Relative path to Kompot file containing P-T information
N_rays	Number of simulated light rays in the atmosphere
RADIUS_PLANET	Radius of the simulated planet/moon in metres
RADIUS_STAR	Radius of the host star in metres
CROSSSECTION_MODE	Whether UV (from Kompot) or IR (from ExoMolOP) crosssections should be used
EXOMOLOP_CROSSSECTION_FOLDER	Relative path containing ExoMolOP infrared crosssections

Table B.1.: KompotSpec configurable parameters, description and valid data types / values

C. KompotSpec development & packages

A list of used packages/libraries is provided in Table C.1. *Pandas* was mainly used for I/O operations for both reading the input files and writing the output files. For reasons including its lackluster performance, *Pandas* dataframes were converted to *numpy* arrays for the radiative transfer calculations. *numpy* was also utilized to vectorize calculations, improving performance. Still, the code is not as efficient as desired, since it is a work-in-progress and full optimization was not the goal of this work. Extensive use of the *Matplotlib* library was made for the figures in Chapter 4.

While the code is working well and producing all the needed outputs, it is not very efficient. This is in large part due to many nested loops and only sporadic vectorization using *numpy*, because the priority of this work was a proof-of-concept on how Kompot's output can be transformed into transit spectra. Code optimization is one of the most glaring areas where the code can be improved in the future (other prospects in Section 5.3.

Package	**Description**
os	General I/O operations for creating folders
shutil	Helper functions for copying files
re	Regular expressions
tqdm	Progress bars to visualize simulation progress
itertool	Avoid nested loop code clutter (does not improves performance)
datetime	Addition of timestamps to simulation files
h5py	Used for accesing ExoMolOP crosssection data in *.h5* format
numpy	Universal math library, improves performance for vectorized calculations
pandas	Reads/Outputs different file types, easy manipulation of
matplotlib	Used for all output flots of KompotSpec

Table C.1.: KompotSpec used packages

The code is currently stored in a private GitHub repository, to which the supervisor is permitted access to. If you are interested in accessing the code, please contact the supervisor found on the title page of this work.

D. Kompot atmospheric composition: Earth model

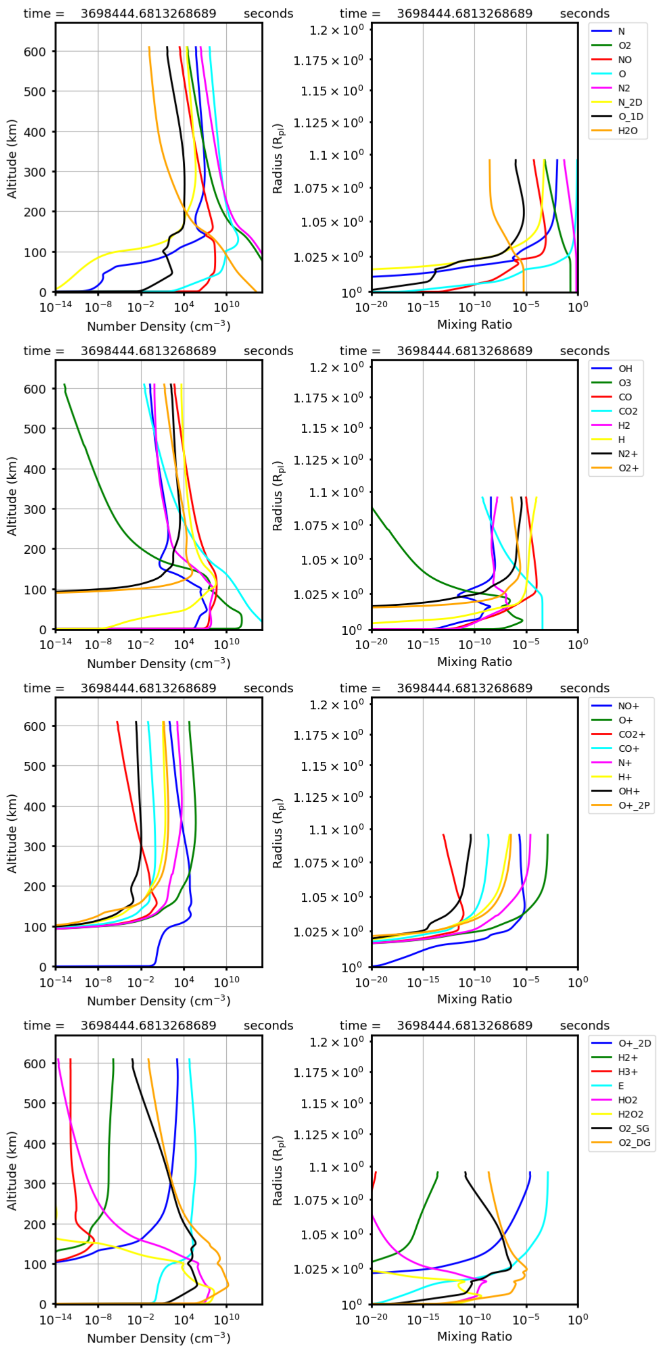

Figure D.1.: Kompot Earth model's atmospheric composition [1 of 4]

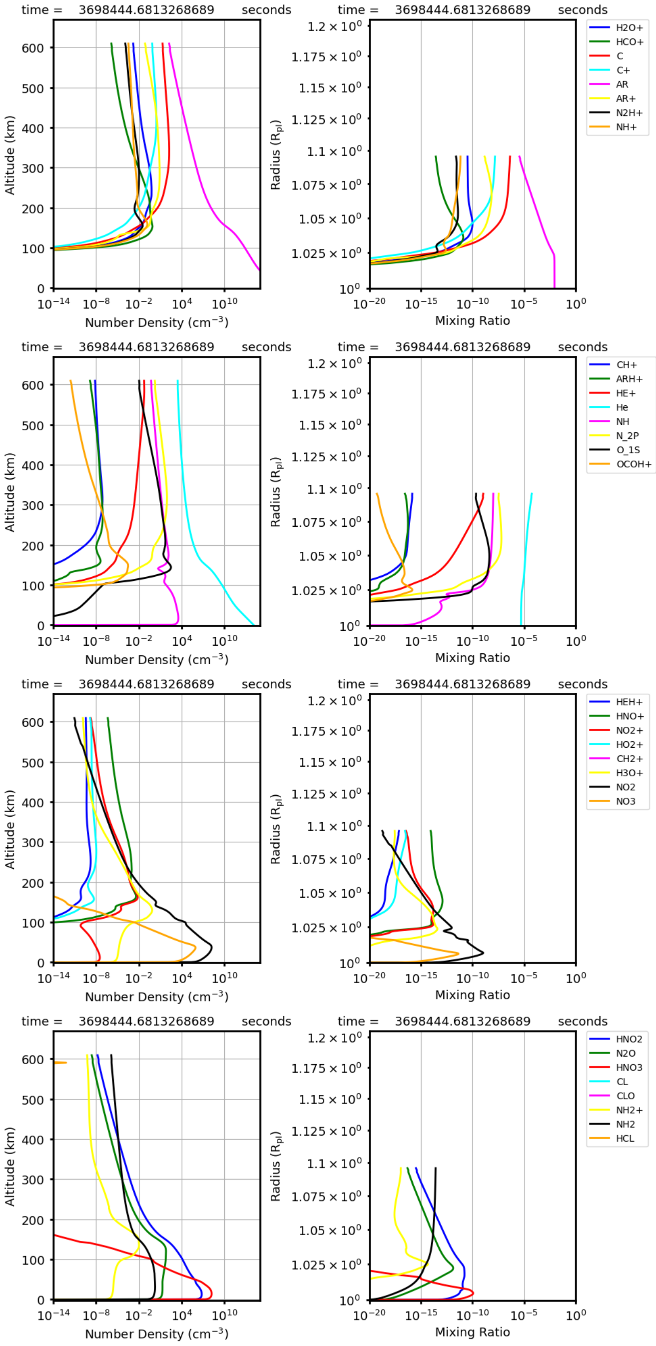

Figure D.2.: Kompot Earth model's atmospheric composition [2 of 4]

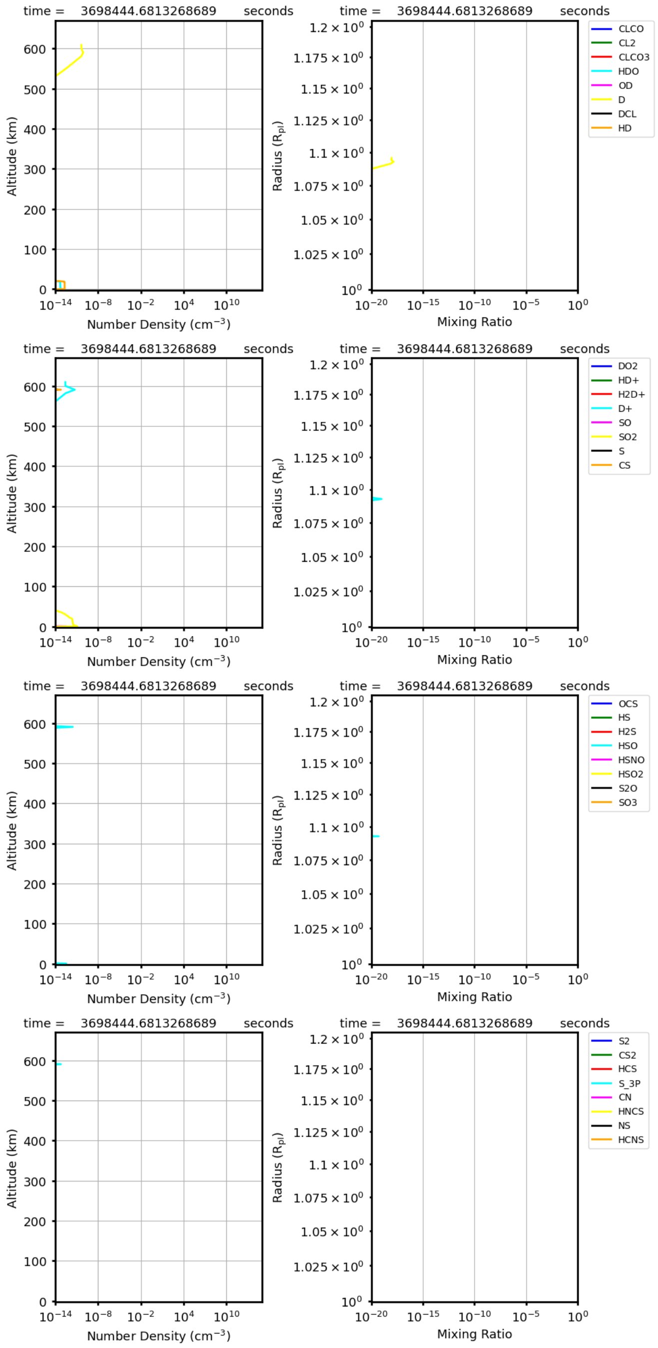

Figure D.3.: Kompot Earth model's atmospheric composition [3 of 4]

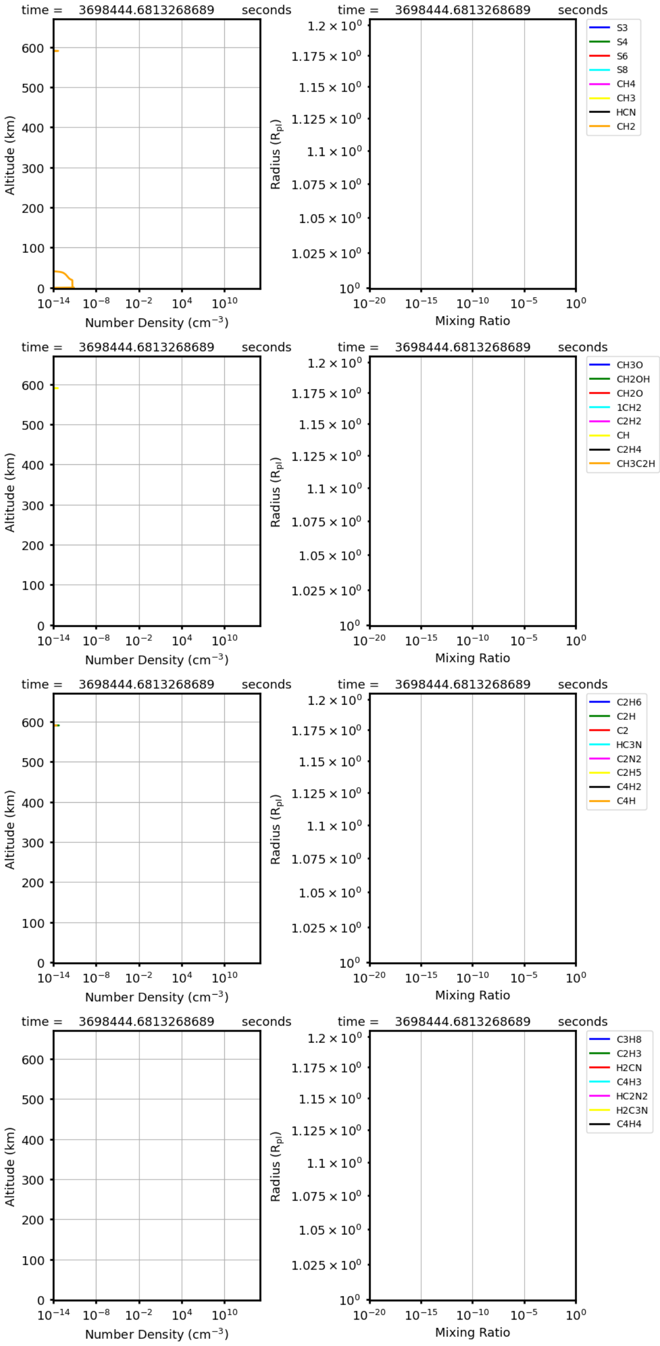

Figure D.4.: Kompot Earth model's atmospheric composition [4 of 4]

E. Kompot atmospheric composition: Titan model

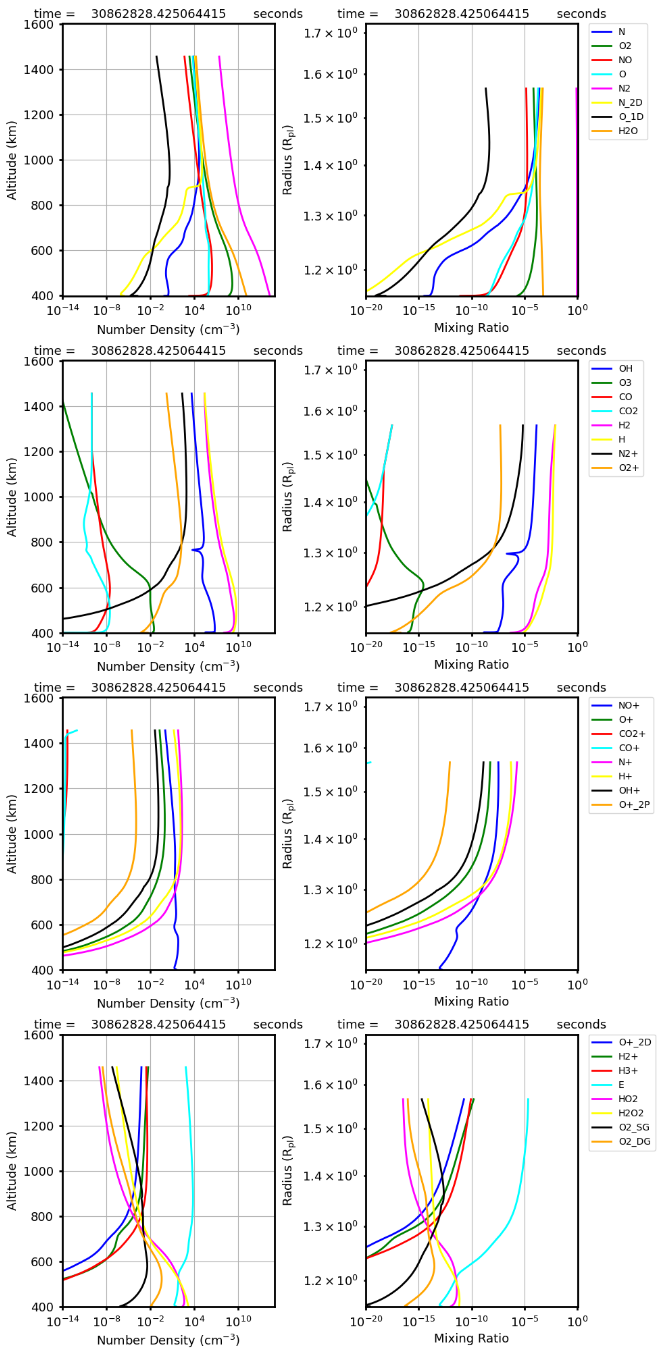

Figure E.1.: Kompot Titan model's atmospheric composition [1 of 4]

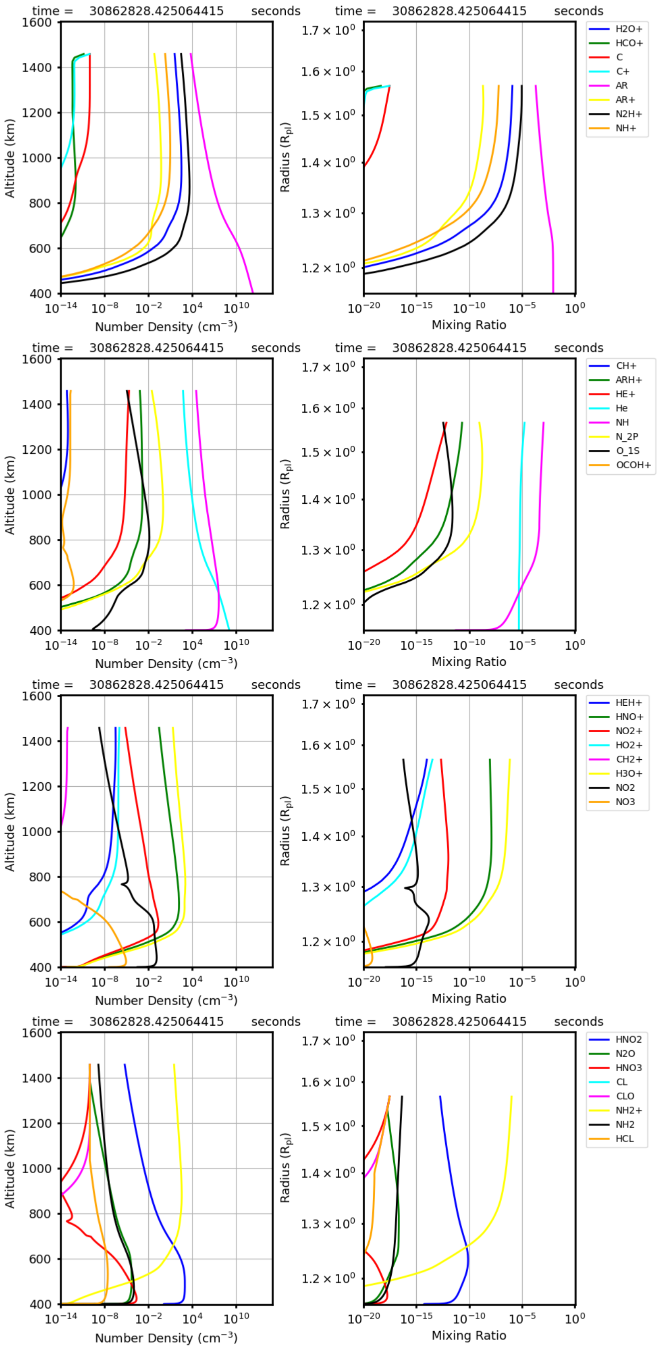

Figure E.2.: Kompot Titan model's atmospheric composition [2 of 4]

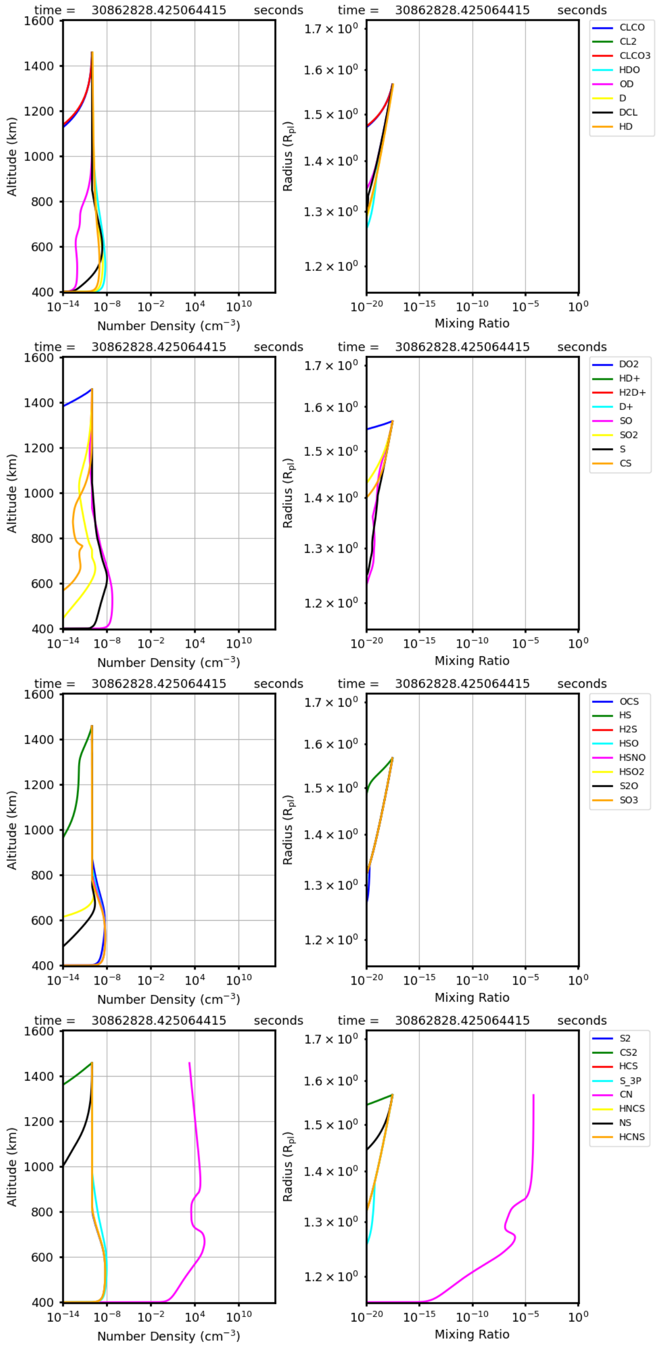

Figure E.3.: Kompot Titan model's atmospheric composition [3 of 4]

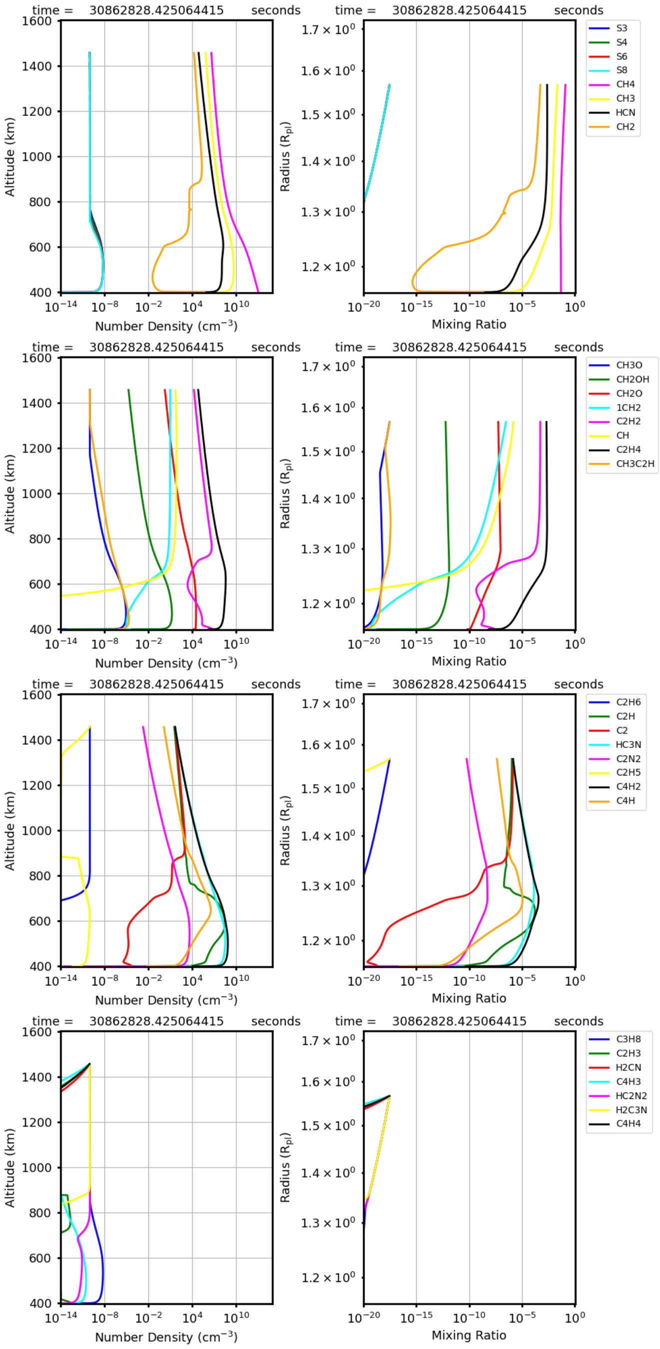

Figure E.4.: Kompot Titan model's atmospheric composition [4 of 4]